Source details

Physical Review D

Formerly known as: Physical Review D - Particles, Fields, Gravitation and Cosmology

Years currently covered by Scopus: 1989, from 2001 to 2003, 2008, from 2015 to 2026

Publisher: American Physical Society

ISSN: 2470-0010 E-ISSN: 2470-0029

Subject area: Physics and Astronomy: Nuclear and High Energy Physics

Source type: Journal

CiteScore 2025
9.0

SJR 2025
1.272

SNIP 2025
1.236

View all documents > | Set document alert | Save to source list

CiteScore | CiteScore rank & trend | Scopus content coverage

CiteScore 2025

$$9.0 = \frac{155{,}535 \text{ Citations } 2022 - 2025}{17{,}373 \text{ Documents } 2022 - 2025}$$

Calculated on 05 May, 2026

CiteScoreTracker 2026

$$8.8 = \frac{153{,}967 \text{ Citations to date}}{17{,}569 \text{ Documents to date}}$$

Last updated on 05 November, 2026 • Updated monthly

CiteScore rank 2025

Category	Rank	Percentile
Physics and Astronomy └ Nuclear and High Energy Physics	#7/97	93rd

View CiteScore methodology > | CiteScore FAQ > | Add CiteScore to your site

About Scopus

What is Scopus

Content coverage

Scopus blog

Scopus API

Privacy matters

Language

日本語版を表示する

查看简体中文版本

查看繁體中文版本

Просмотр версии на русском языке

Customer Service

Help

Tutorials

Contact us

ELSEVIER

Terms and conditions Privacy policy Cookies settings

All content on this site: Copyright © 2026 Elsevier B.V., its licensors, and contributors. All rights are reserved, including those for text and data mining, AI training, and similar technologies. For all open access content, the relevant licensing terms apply.

RELX™

SCImago Journal & Country Rank

Journal Rankings | Journal Value | Country Rankings | Viz Tools | About Us | Search

Physical Review D

United States | Universities and research institutions | Media Ranking

Country
United States

SCImago Institutions Rankings

SCImago Media Rankings

Subject Area and Category
Physics and Astronomy
- Nuclear and High Energy Physics
- Physics and Astronomy (miscellaneous)

Publisher
American Physical Society

SJR 2025
1.272 Q1

H-Index
424

Publication type
Journals

ISSN
24700010, 24700029

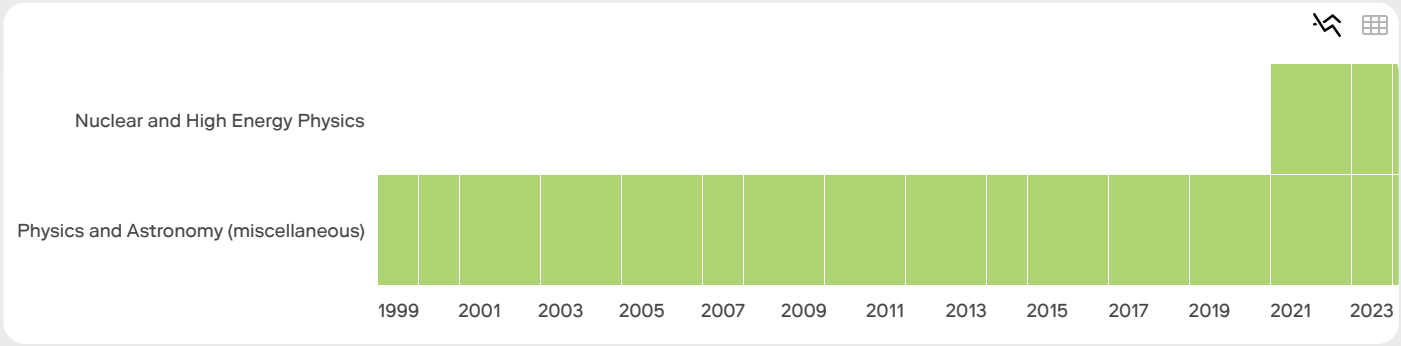
Coverage
1989, 2001-2003, 2008, 2015-2026

Information
Home
How to publish in this journal
prd@aps.org

Scope
Physical Review D (PRD) is a leading journal in elementary particle physics, field theory, gravitation, and cosmology and is one of the top-cited journals in high-energy physics.

PRD covers experimental and theoretical results in all aspects of particle physics, field theory, gravitation and cosmology, including: Particle physics experiments, Electroweak interactions, Strong interactions, Lattice field theories, lattice QCD, Beyond the standard model physics, Phenomenological aspects of field theory, general methods, Gravity, cosmology, cosmic rays, Astrophysics and astroparticle physics, General relativity, Formal aspects of field theory, field theory in curved space, String theory, quantum gravity, gauge/gravity duality.

Quartiles



Find similar journals

All quartiles | All countries | All subject categories | Clear filters | Download

Only Open Access Journals

1 - General Relativity and Gravitation

84%

similarity

2 - Physics of the Dark Universe

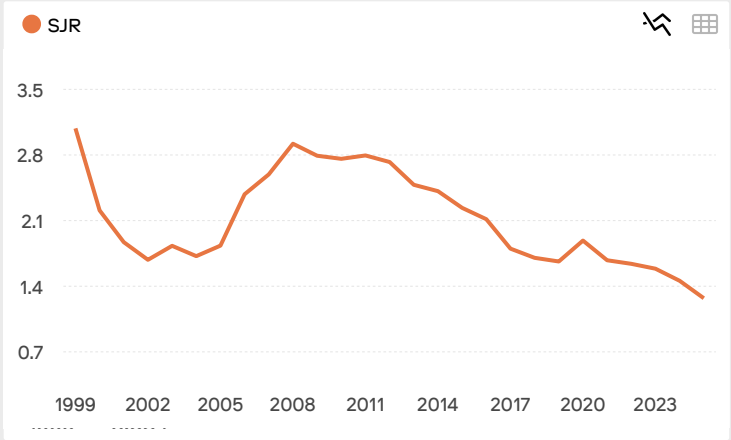
83%

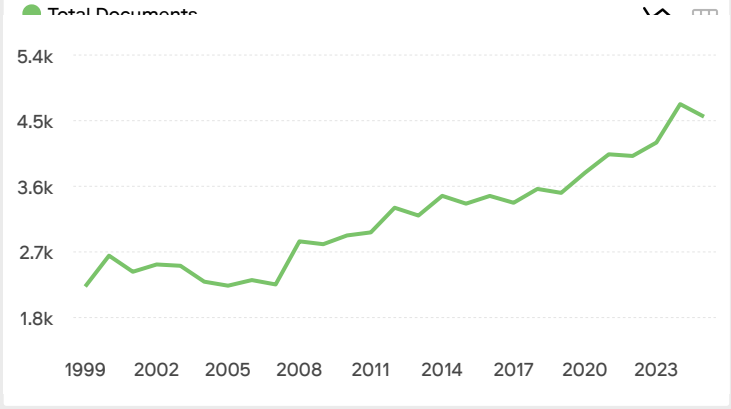
similarity

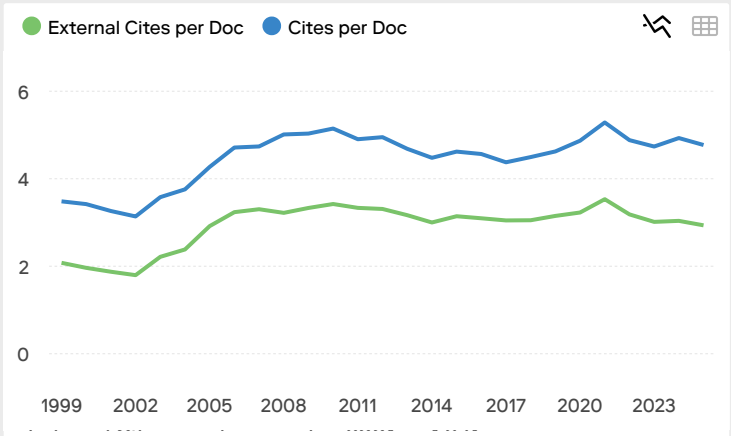
3 - International Journal of Modern Physics D

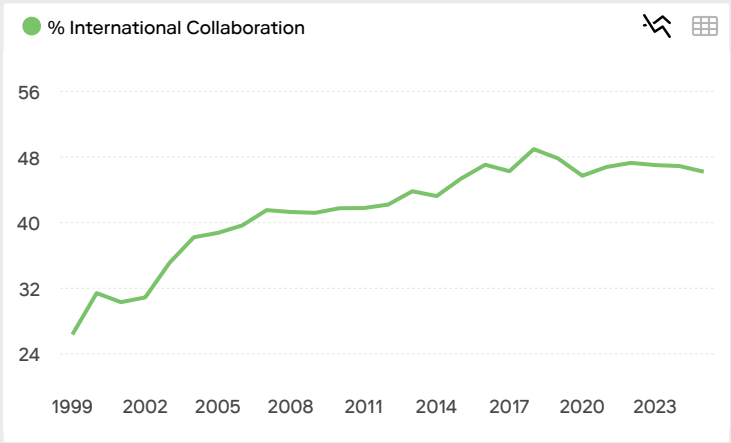
82%

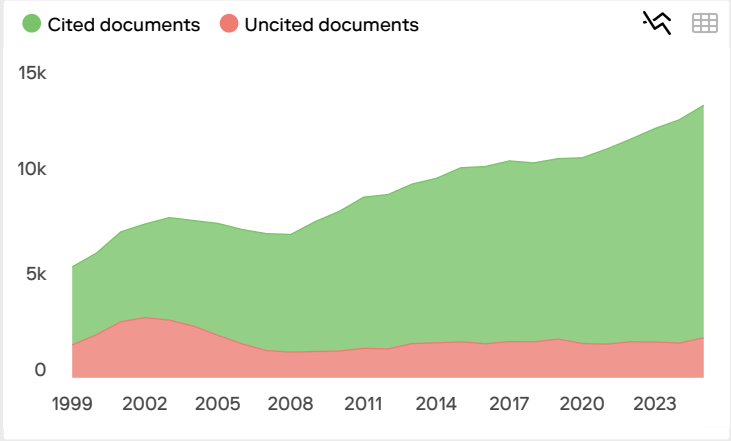
similarity




Total Documents
5.4k
4.5k
3.6k
2.7k
1.8k
1999
2002
2005
2008
2011
2014
2017
2020
2023

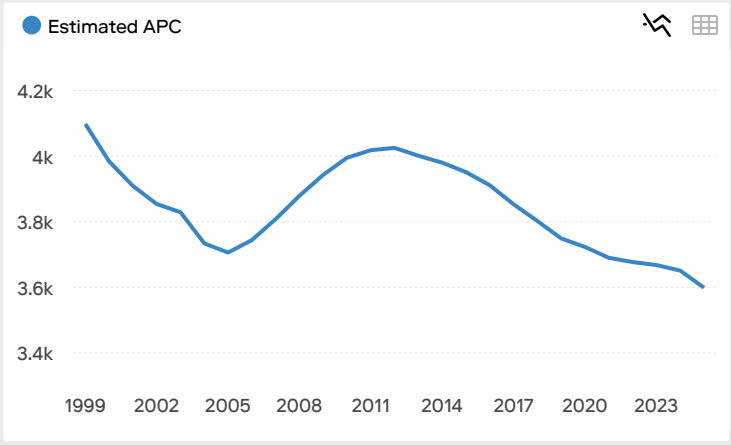

External Cites per Doc
Cites per Doc
6
4
2
0
1999
2002
2005
2008
2011
2014
2017
2020
2023

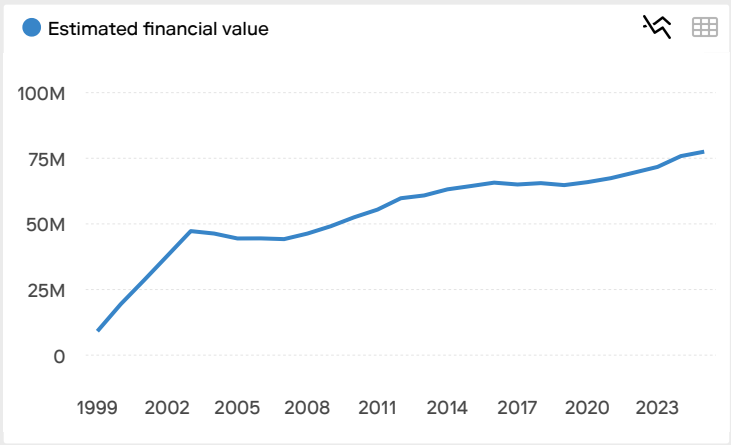

% International Collaboration
56
48
40
32
24
1999
2002
2005
2008
2011
2014
2017
2020
2023

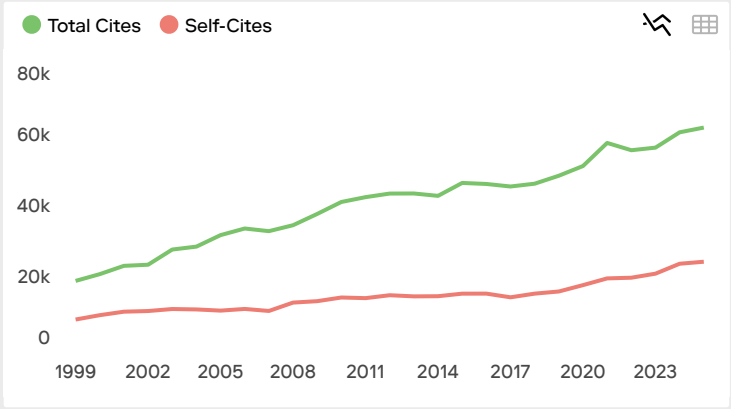

Cited documents
Uncited documents
15k
10k
5k
0
1999
2002
2005
2008
2011
2014
2017
2020
2023


% Female Authors

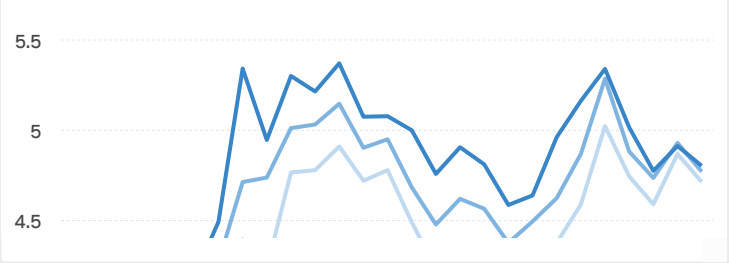


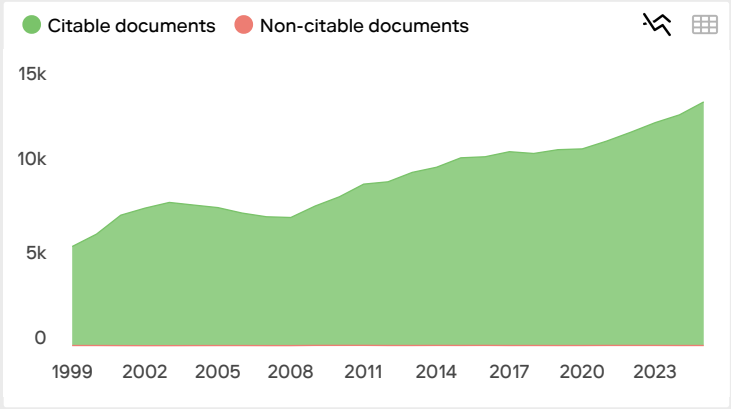


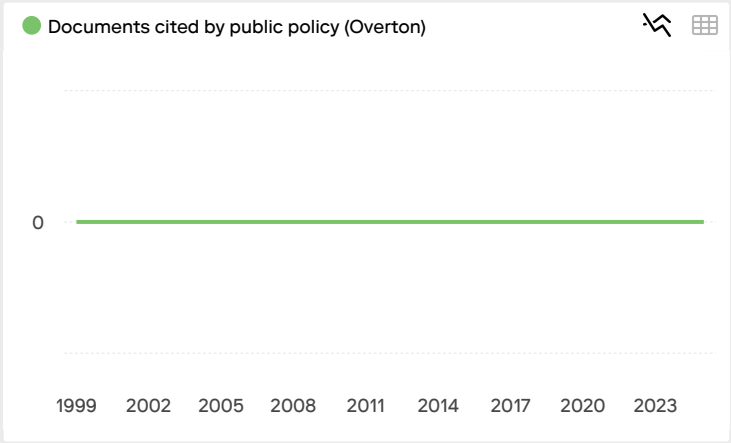


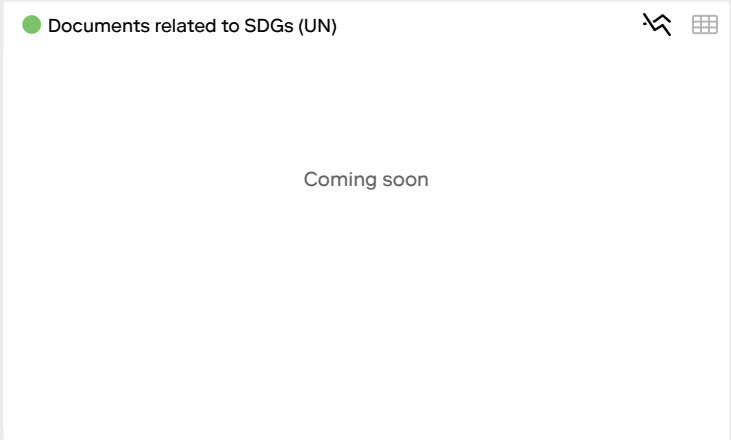


Citations per document











Show this widget in your own website

Just copy the code below and paste within your html code:

```
<a href="https://www.scimago
```

SCImago Graphica

Explore, visually communicate and make sense of data with our new data visualization tool.



Metrics based on Scopus® data as of March 2026

H

Hans hammann

11 months ago

Hallö, ich habe eine neue Theorie entwickelt ," raumenergie", die umgekehrt zu Newton funktioniert aber nur in kosmischen skalen und die auch die Rotation an galaxienraendern erklaert, sowie die expansion des Universums. Interesse? Danke!

reply

Melania Ortiz - SCImago Team

10 months ago

Dear Hans,
Thank you for contacting us.
We are sorry to tell you that SCImago Journal & Country Rank is not a journal. SJR

is a portal with scientometric indicators of journals indexed in Elsevier/Scopus. We suggest you visit the journal's homepage (See submission/author guidelines) or contact the journal's editorial staff , so they could inform you more deeply. Best Regards, SCImago Team

P

patrizia vitale

7 years ago

Hello,

my institution uses the SJR for bibliometric purposes. Physical Review D and other APS journals have changed their ISSN through the years. It appears that this is not correctly handled by SJR: For example, if I enter the ISSN code of Phys. Rev D for the year 2014, which is 1550-7998, in your dialog box above, I get no answer.
This implies that papers published on PRD prior to 2015 get 0 as SJR ranking.
Could you address this issue, which is very important for the correct evaluation of our research?
Thank you very much.

reply

Melanie Ortiz

7 years ago

Dear Patrizia,
SJR is a portal with scientometric indicators of journals indexed in Scopus. SJR has no authority over the data of the journals; they are the ones that Scopus sends us. The metadata are property of Scopus. SCImago has a signed agreement that limits our performance to the generation of scientometric indicators derived from the metadata sent in the last update. We suggest that you contact Scopus through this link to report the inconsistencies or modifications that you want to make in SCImago: https://service.elsevier.com/app/answers/detail/a_id/14883/kw/scimago/supporthub/scopus/. Best Regards, SCImago Team

Name

Email

Message

I'm not a robot reCAPTCHA

Send

The users of Scimago Journal & Country Rank have the possibility to dialogue through comments linked to a specific journal. The purpose is to have a forum in which general doubts about the processes of publication in the journal, experiences and other issues derived from the publication of papers are resolved. For topics on particular articles, maintain the dialogue through the usual channels with your editor.

SCImago Journal & Country Rank

Services

Journal Rankings
Country Rankings
Journal Value

About us

Who we are
Contact us

SCImago's products

SCImago Journal Country & Rank
SCImago Institutions Ranking
SCImago Media Ranking
SCImago Iber
SCImago Arab
SCImago Graphica
Ediciones Profesionales de la Información

All the information shown in the SCImago Journal Country & Rank website can be used for non-commercial purposes as long as it is cited.

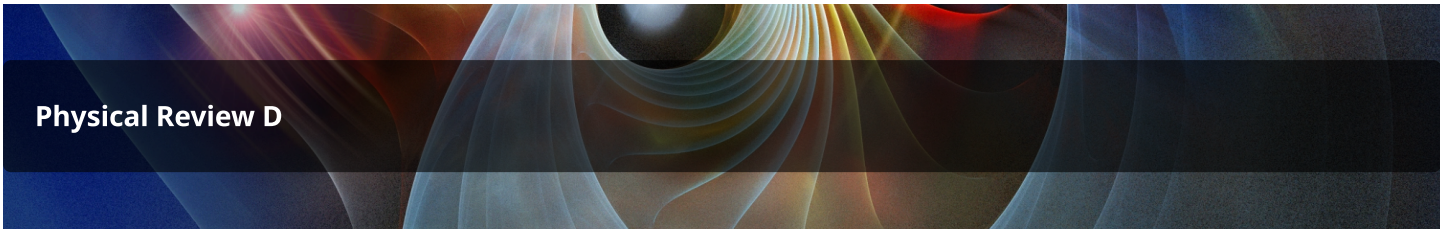
How to cite:

SCImago, (n.d.). SJR-SCImago Journal Country & Rank [Portal]. Retrieved (Date), from https://www.scimagojr.com

Powered by:
Scopus®

© 2026 SCImago Journal & Country Rank Legal Notice Privacy Policy Accessibility

APS Journals



Browse Issues: Prev Next

Volume 114, Issue 9 (partial)

1 November 2026

LETTERS

LETTER

Measurement of $Z\gamma$ production in proton-proton collisions at $\sqrt{s} = 13.6$ TeV and constraints on neutral triple gauge couplings

A. Hayrapetyan *et al.* (CMS Collaboration)

Phys. Rev. D **114**, L091101 (2026) - Published 13 November, 2026

LETTER

Constraining the neutrino-nucleon cross section with the ultrahigh-energy KM3NeT event

Toni Bertólez-Martínez and Dan Hooper

Phys. Rev. D **114**, L091701 (2026) - Published 9 November, 2026

LETTER

Universal seesaw mechanism for fermion masses and strong CP problem

Pavel Fileviez Pérez and Clara Murgui

Phys. Rev. D **114**, L091702 (2026) - Published 12 November, 2026

ARTICLES

Improved search for $\psi(3770) \to \gamma\eta_c(1S, 2S)$ radiative transitions

M. Ablikim *et al.* (BESIII Collaboration)

Phys. Rev. D **114**, 092001 (2026) - Published 3 November, 2026

Measurements of absolute branching fractions of $D^{0(+)} \to KKK\pi$ decays

M. Ablikim *et al.* (BESIII Collaboration)

Phys. Rev. D **114**, 092002 (2026) - Published 5 November, 2026

ANUBIS detector and its sensitivity to neutral long-lived particles

Thomas Adolphus *et al.* (ANUBIS Collaboration)

Phys. Rev. D **114**, 092003 (2026) - Published 6 November, 2026

DMRadio-Core: A new approach for GUT-scale axion searches

V. Ankel *et al.*

Phys. Rev. D **114**, 092004 (2026) - Published 5 November, 2026

Background of the BULLKID detector array operated with a moderate shield on the surface

D. Delicato *et al.*

Phys. Rev. D **114**, 092005 (2026) - Published 6 November, 2026

Suppression of $^{14}\mathrm{C}$ photon hits in large liquid scintillator detectors via spatiotemporal deep learning

Junle Li, Zhaoxiang Wu, Guanda Gong, Zhaohan Li, Wuming Luo, Jiahui Wei, Wenxing Fang, and Hehe Fan

Phys. Rev. D **114**, 092006 (2026) - Published 9 November, 2026

Deep-learning-based low-energy trigger algorithms for the Hyper-Kamiokande experiment

Katharina Lachner, Saúl Alonso-Monsalve, Benjamin Richards, and Davide Sgalaberna

Phys. Rev. D **114**, 092007 (2026) - Published 10 November, 2026

First full physics benchmark for highly granular calorimeter surrogates

Thorsten Buss, Henry Day-Hall, Frank Gaede, Gregor Kasieczka, Katja Krüger, Anatolii Korol, Thomas Madlener, and Peter McKeown

Phys. Rev. D **114**, 092009 (2026) - Published 13 November, 2026

Revisiting $\bar{B}^0 \to \Lambda_c^+ \bar{p}$ decay with higher twist corrections

Zhi-Tian Zou, Ying Li, and Zhou Rui

Phys. Rev. D **114**, 093001 (2026) - Published 4 November, 2026

Physical Review D

Sign up for email alerts

Journal

Phys. Rev. D **114**, 093003 (2026) - Published 10 November, 2026

PURPOSE-LED PUBLISHING™
SCIENCE IS OUR ONLY SHAREHOLDER

ρ mesons in finite magnetic field and finite temperature

Zhiyang Liu, Min Zhou, Yvming Tian, Rui Zhou, Guoyun Shao, and Shijun Mao

Phys. Rev. D **114**, 094001 (2026) - Published 3 November, 2026

Authors

Reviewers

Librarians

Students

Connect

Proton-Omega bound state revisited via the Pomeron exchange model

Yu-Jie Feng, Qian Wang, and Qiang Zhao

Phys. Rev. D **114**, 094002 (2026) - Published 3 November, 2026

Meson octet in a uniform magnetic field

Prabal Adhikari

Phys. Rev. D **114**, 094003 (2026) - Published 3 November, 2026
ISSN 2470-0029 (online), 2470-0010 (print).

©2026 American Physical Society. All rights reserved.
Physical Review D™ is a trademark of the American Physical Society registered in the United States, Canada, European Union, and Japan. The *APS Physics logo* and *Physics logo* are trademarks of the American Physical Society. Information about registration may be found here. Use of the American Physical Society websites and journals implies that the user has read and agrees to our Terms and Conditions and any applicable Subscription Agreement.

Photon emission from rotating plasmas: A generalized McLerran-Toimela formula and the onset of superradiance

Kirill Tuchin

Phys. Rev. D **114**, 094004 (2026) - Published 4 November, 2026

Updated analysis of charmonium states in a relativized quark potential model

Xiu-Li Gao, Jun-Xi Cui, Yu-Hui Zhou, and Zhi-Yong Zhou

Phys. Rev. D **114**, 094005 (2026) - Published 4 November, 2026

Bayesian inference of the magnetic component in the quark-gluon plasma

Yu Guo, Jinfeng Liao, and Shuzhe Shi

Phys. Rev. D **114**, 094006 (2026) - Published 4 November, 2026

Next-to-leading-order QCD corrections to the radiative decays $\chi_{bJ} \to J/\psi + \gamma$

Yu-Dong Zhang and Zai-Fu Jiang

Phys. Rev. D **114**, 094007 (2026) - Published 6 November, 2026

Two-variable longitudinal distribution of the Λ_b in a three-quark light-front model

Shuai Xu and Xiao-Nan Li

Phys. Rev. D **114**, 094008 (2026) - Published 9 November, 2026

$D^*D^*\pi$ and $B^*B^*\pi$ couplings from light-cone sum rules

Chao Wang

Phys. Rev. D **114**, 094009 (2026) - Published 9 November, 2026

Tensor-polarized parton distribution functions of the deuteron by a convolution model

S. Kumano and Kenshi Kuroki

Phys. Rev. D **114**, 094010 (2026) - Published 9 November, 2026

Baryon enhancement in jets

Antonio Ortiz and Róbert Vértesi

Phys. Rev. D **114**, 094011 (2026) - Published 12 November, 2026

Ω_c baryon spectrum and strong decays in a constituent quark model

Hui-Hua Zhong, Ming-Sheng Liu, Li-Ye Xiao, Kai-Lei Wang, Qi Li, and Xian-Hui Zhong

Phys. Rev. D **114**, 094012 (2026) - Published 12 November, 2026

Scalar and spin polarizabilities of singly heavy baryons within heavy baryon chiral perturbation theory

Zi-Jun Li, Zhan-Wei Liu, and Ping Chen

Phys. Rev. D **114**, 094013 (2026) - Published 12 November, 2026

New look at the X compositeness from its lineshape

A. Carducci, G. Cianti, P. D'Annibali, D. Germani, and A. D. Polosa

Phys. Rev. D **114**, 094014 (2026) - Published 13 November, 2026

λ, ρ, and σ Regge trajectories for the hexaquark $(\bar{u}(cc))(b(\bar{b}\bar{b}))$ in the triquark-antitriquark picture

Xin-Ru Liu, Qi Liu, and Jiao-Kai Chen

Phys. Rev. D **114**, 094015 (2026) - Published 13 November, 2026

Investigating three-body resonances in $\alpha\alpha\Omega/\Omega_{ccc}$ clusters within the ${}^{9}_{\Omega/\Omega_{ccc}}$Be nucleus

Hao Zhou and Xiang Liu

Phys. Rev. D **114**, 094016 (2026) - Published 13 November, 2026

Probing SU(2) quark flavor asymmetry with W bosons at RHIC

Maximiliano Ponce-Chavez

Phys. Rev. D **114**, 094017 (2026) - Published 13 November, 2026

Forward hadron production in pp collisions at LHC energies from an event generator based on the color glass condensate framework

Hirotsugu Fujii, Tetsufumi Hirano, Kazunori Itakura, Yasushi Nara, and Shujun Zhao

Phys. Rev. D **114**, 094018 (2026) - Published 13 November, 2026

Properties of the $D_{s0}^{*}(2317)^{\pm}$ in hot and dense nuclear matter

Tomona Kinugawa, Àngels Ramos, and Laura Tolos

Phys. Rev. D **114**, 094019 (2026) - Published 13 November, 2026

Revisiting the $\Lambda(1405)$ pole structure with convolutional neural networks

Julius B. Pagayon, Vince Angelo A. Chavez, and Denny Lane B. Sombillo

Phys. Rev. D **114**, 094020 (2026) - Published 13 November, 2026

Magnetic moments of decuplet baryons in isospin asymmetric magnetized strange matter

Hrishika P, Manpreet Kaur, Suneel Dutt, Harleen Dahiya, and Arvind Kumar

Phys. Rev. D **114**, 094021 (2026) - Published 13 November, 2026

Static quark-antiquark interactions in rotating SU(3) gluodynamics

Heng-Tong Ding, Olaf Kaczmarek, Ran Luo, and Hai-Tao Shu

Phys. Rev. D **114**, 094501 (2026) - Published 4 November, 2026

Hamiltonian lattice QED_3 with one and two flavors of Wilson fermions: Topological structure and response

Sriram Bharadwaj, Emil Rosanowski, Simran Singh, Alice Di Tucci, Changnan Peng, Karl Jansen, Lena Funcke, and Di Luo

Phys. Rev. D **114**, 094502 (2026) - Published 5 November, 2026

Heavy-meson bag parameters using gradient flow

Matthew Black, Robert V. Harlander, Jonas T. Kohnen, Fabian Lange, Antonio Rago, Andrea Shindler, and Oliver Witzel

Phys. Rev. D **114**, 094503 (2026) - Published 5 November, 2026

Structure of $\mathrm{QC_2D}$ ground state fields at nonzero matter densities

Ragib F. Hasan, Matthew Cummins, Waseem Kamleh, Dale Lawlor, Derek B. Leinweber, Ian van Schalkwyk, and Jon-Ivar Skullerud

Phys. Rev. D **114**, 094504 (2026) - Published 5 November, 2026

Radiative decays of the h_c meson from lattice QCD

Mischa Batelaan, Jozef J. Dudek, and Robert G. Edwards (for the Hadron Spectrum Collaboration)

Phys. Rev. D **114**, 094505 (2026) - Published 6 November, 2026

Path optimization method for the sign problem: Insights from random matrix models

Kouji Kashiwa, Yusuke Namekawa, and Hayato Takase

Phys. Rev. D **114**, 094506 (2026) - Published 13 November, 2026

Quantum simulation of QCD in axial gauge

Xiaojun Yao

Phys. Rev. D **114**, 094507 (2026) - Published 13 November, 2026

Precision tests of SM and new physics with the COHERENT Ge-mini and TEXONO data

Tousib Ahmed, Ayan Chattaraj, Anirban Majumdar, Newton Nath, and Rahul Srivastava

Phys. Rev. D **114**, 095001 (2026) - Published 2 November, 2026

Crossing into the $m_a > f_a$ region for leptophilic ALPs

Marta F. Zamoro, Álvaro Lozano-Onrubia, Luca Merlo, and Samuel Rosende Herrero

Phys. Rev. D **114**, 095002 (2026) - Published 2 November, 2026

Freeze-in $SU(2)$ vector dark matter at low reheating temperature

Dilip Kumar Ghosh, Sourav Gope, Xiao-Gang He, Xuan Hong, and Sk Jeesun

Phys. Rev. D **114**, 095003 (2026) - Published 3 November, 2026

Semileptonic sum rules in heavy-to-light charm decays

Motoi Endo, Syuhei Iguro, Satoshi Mishima, Takeru Uchiyama, and Ryoutaro Watanabe

Phys. Rev. D **114**, 095004 (2026) - Published 2 November, 2026

Complementary probes of bilinear R-parity violating SUSY models with a winolike LSP via neutrino oscillations and at the LHC

Arghya Choudhury and Arpita Mondal

Phys. Rev. D **114**, 095005 (2026) - Published 2 November, 2026

Radiative lifting of $\mathbb{Z}_3$ domain-wall degeneracy in a type-III seesaw model: Implications for leptogenesis and gravitational waves

Priya, Labh Singh, B. C. Chauhan, and Surender Verma

Phys. Rev. D **114**, 095006 (2026) - Published 3 November, 2026

Resonant heterodyne conversion applied to a low-frequency haloscope for dark matter axion searches in the 1–35 MHz range

Jose R. Navarro-Madrid, José Reina-Valero, Alejandro Díaz-Morcillo, and Benito Gimeno

Phys. Rev. D **114**, 095007 (2026) - Published 3 November, 2026

Precision solar system dynamics for ultralight dark matter search

Jonas Frerick, Hyungjin Kim, and Felix Kling

Phys. Rev. D **114**, 095008 (2026) - Published 4 November, 2026

Establishing perturbatively the Kostelecký conjecture in all massive sectors of the standard-model extension

M. D. C. Torri

Phys. Rev. D **114**, 095009 (2026) - Published 5 November, 2026

Testing exotic electron-electron interactions with the helium ionization-energy anomaly

Lei Cong, Filip Ficek, Rinat Abdullin, Mikhail G. Kozlov, and Dmitry Budker

Phys. Rev. D **114**, 095010 (2026) - Published 5 November, 2026

Minimal-length kinematics of coherent light and a proposed two-color vacuum chronoscopy

Zhi-Wei Wang, Saurya Das, and Samuel L. Braunstein

Phys. Rev. D **114**, 095011 (2026) - Published 5 November, 2026

Asymmetric dark matter from low-scale spontaneous leptogenesis

Hiroki Takahashi and Juntaro Wada

Phys. Rev. D **114**, 095012 (2026) - Published 5 November, 2026

Is the conventional picture of coherence time complete? Dark matter recoherence from substructures

Chaitanya Paranjape, Gilad Perez, Wolfram Ratzinger, and Somasundaram Sankaranarayanan

Phys. Rev. D **114**, 095013 (2026) - Published 6 November, 2026

Constraints on a light leptophilic scalar from dark-sector couplings

Marco Graziani, Giacomo Landini, Federico Mescia, Claudio Toni, and Ludovico Vittorio

Phys. Rev. D **114**, 095014 (2026) - Published 9 November, 2026

Searching for symmetric mass generation with staggered fermions in four dimensions

Nouman Butt, Simon Catterall, Gwen Hartshaw, and Anna Hasenfratz

Phys. Rev. D **114**, 095015 (2026) - Published 6 November, 2026

Strong CP phase and the PMNS phase in Dirac left-right symmetry

Vladimir Tello

Phys. Rev. D **114**, 095016 (2026) - Published 6 November, 2026

Constraints on vectorlike top dipole interactions from top-associated photon measurements at the LHC

M. Sahraei, Y. Hosseini, and M. Mohammadi Najafabadi

Phys. Rev. D **114**, 095017 (2026) - Published 6 November, 2026

Small-instanton effects in an atlas of Kim-Shifman-Vainshtein-Zakharov axion models

Ning Chen and Saurabh K. Shukla

Phys. Rev. D **114**, 095018 (2026) - Published 10 November, 2026

Numerical method for the efficient calculation of scattering form factors

Benjamin Lillard, Jack D. Shergold, and Carlos Blanco

Phys. Rev. D **114**, 095019 (2026) - Published 6 November, 2026

Probing quadratically coupled ultralight dark matter with the laser interferometer space antenna

Xucheng Gan, Hyungjin Kim, Anna-Malin Lemke, and Andrea Mitridate

Phys. Rev. D **114**, 095020 (2026) - Published 10 November, 2026

Quantum interferometric probe of neutron-hidden neutron oscillations

A. Capolupo, G. Pisacane, A. Quaranta, and P. Böni

Phys. Rev. D **114**, 095021 (2026) - Published 10 November, 2026

Can $\gamma\gamma$ collisions rival e^-e^+ in probing doubly charged Higgs bosons?

Abdesslam Arhrib, Rachid Benbrik, Mohammed Boukidi, Mohamed Chabab, Khalid Goure, and Stefano Moretti

Phys. Rev. D **114**, 095022 (2026) - Published 10 November, 2026

Higgs-portal Stueckelberg dark matter

Antonio De Felice, Takehiro Ogura, Shinji Tsujikawa, and Kimiko Yamashita

Phys. Rev. D **114**, 095023 (2026) - Published 10 November, 2026

Exotic Higgs decays at a muon collider

JiJi Fan, Lingfeng Li, Tao Liu, Yanhan Wang, and Mingrui Zhou

Phys. Rev. D **114**, 095024 (2026) - Published 13 November, 2026

Updated constraints on a long-lived X_{17} vector boson

A. Celentano, A. Marini, and L. Marsicano

Phys. Rev. D **114**, 095025 (2026) - Published 12 November, 2026

Enhanced cosmic-ray cooling in AGN from dark matter deep inelastic scattering

Linjie Li, Chih-Ting Lu, Arvind Kumar Mishra, Liangliang Su, and Lei Wu

Phys. Rev. D **114**, 095026 (2026) - Published 12 November, 2026

$b \to c\bar{u}q$ decay and CP violating observables in the presence of new physics contributions

Xuanning Guo, Albertus Hariwangsa Panuluh, Hiroyuki Umeeda, and Jinglong Zhu

Phys. Rev. D **114**, 095027 (2026) - Published 13 November, 2026

Inelastic scattering effects on attenuation of boosted dark matter

Guanhua Gu, Liangliang Su, Lei Wu, and Jin Min Yang

Phys. Rev. D **114**, 095028 (2026) - Published 13 November, 2026

Baryogenesis induced by magnetic fields during the electroweak phase transition

transition

Yuefeng Di, Ligong Bian, and Rong-Gen Cai

Phys. Rev. D **114**, 095029 (2026) - Published 13 November, 2026

Higgs boson production classifier using weak supervision

Kai-Feng Chen, Yi-An Chen, Cheng-Wei Chiang, and Feng-Yang Hsieh

Phys. Rev. D **114**, 096001 (2026) - Published 3 November, 2026

Photon production from gluon splitting and fusion induced by a magnetic field of arbitrary strength in relativistic heavy-ion collisions

Alejandro Ayala, Santiago Bernal-Langarica, José Jorge Medina-Serna, and Ana Julia Mizher

Phys. Rev. D **114**, 096002 (2026) - Published 3 November, 2026

Spin entanglement signatures of proton from a light-front Hamiltonian

Chen Qian, Siqi Xu, Yang-Guang Yang, and Xingbo Zhao

Phys. Rev. D **114**, 096003 (2026) - Published 4 November, 2026

Taming symbolic integration-by-parts reduction with intermediate bases

Qian Song

Phys. Rev. D **114**, 096004 (2026) - Published 4 November, 2026

Analytic results for the two-loop renormalization constants of Feynman gauge QED

Gregory S. Adkins, Elias Mitchell, and A. Volkan Turan

Phys. Rev. D **114**, 096005 (2026) - Published 10 November, 2026

Phenomenological revisit of the $B \to \pi\pi$ decays by incorporating soft color-octet contributions

Yueling Yang, Bingbing Yang, and Junfeng Sun

Phys. Rev. D **114**, 096006 (2026) - Published 9 November, 2026

Non-Markovian heavy-quark equilibration and equilibrium correlation function in a thermal medium

Monisha Nair, Juan M. Torres-Rincon, and Santosh K. Das

Phys. Rev. D **114**, 096007 (2026) - Published 9 November, 2026

Electromagnetic form factors of singly charmed baryons Σ_c and Λ_c in a covariant quark-diquark model

Ye Cao, Cheng Chen, Dongyan Fu, and Ju-Jun Xie

Phys. Rev. D **114**, 096008 (2026) - Published 10 November, 2026

Beyond leading-logarithm photon production from two-loop diagrams in a hot QCD medium

Sumit, Ritesh Ghosh, and Munshi G. Mustafa

Phys. Rev. D **114**, 096009 (2026) - Published 10 November, 2026

Revisiting curvature corrections for field theory cosmic strings

Josu C. Aurrekoetxea, Jose J. Blanco-Pillado, Alberto García Martín-Caro, and J. M. Queiruga

Phys. Rev. D **114**, 096010 (2026) - Published 10 November, 2026

Electric field fluctuations and renormalization group flows in a self-interacting scalar field theory

Melanie Martínez Villarreal, Enrique Muñoz, and Marcelo Loewe

Phys. Rev. D **114**, 096011 (2026) - Published 12 November, 2026

Lorentz violation and vector meson dominance

Brett Altschul

Phys. Rev. D **114**, 096012 (2026) - Published 12 November, 2026

Spin-resolved decay of axionlike particles into electron-positron pairs in strong electromagnetic fields

Xiaodan Mao, Yue-Yue Chen, and Pei-Lun He

Phys. Rev. D **114**, 096013 (2026) - Published 13 November, 2026

Resolving the twofold ambiguity in τ momentum reconstruction via a self-consistent weighting method

Rong-Gang Ping

Phys. Rev. D **114**, 096014 (2026) - Published 13 November, 2026

Investigating the P-wave DK^* molecular interpretation of the $D_{s1}(2700)$ via its strong decays

Qing Lu, ZheHao Zhu, Yin Huang, and Cai Cheng

Phys. Rev. D **114**, 096015 (2026) - Published 13 November, 2026

ERRATA

Erratum: Probing new physics and CP violation in $\nu_\tau n \to \Lambda_c \tau^- (\pi^- \nu_\tau)$ and $\bar{\nu}_\tau p \to \Lambda \tau^+ (\pi^+ \bar{\nu}_\tau)$ [Phys. Rev. D 113, 095005 (2026)]

E. Hernández, J. Nieves, and J. E. Sobczyk

Phys. Rev. D **114**, 099901 (2026) - Published 4 November, 2026

$b \to c\bar{u}q$ decay and *CP* violating observables in the presence of new physics contributions

Xuanning Guo,[1,*] Albertus Hariwangsa Panuluh,[2,†] Hiroyuki Umeeda,[1,‡] and Jinglong Zhu[1,§]

[1]*Center for Theoretical Physics and College of Physics, Jilin University, Changchun 130012, China*
[2]*Department of Physics Education, Faculty of Teacher Training and Education, Sanata Dharma University, Paingan, Maguwohardjo, Sleman, Yogyakarta 55282, Indonesia*

(Received 1 June 2026; accepted 7 October 2026; published 13 November 2026)

In this work, a comprehensive analysis for processes related to $b \to c\bar{u}q(q = d, s)$ transitions is carried out, including new physics contributions. In light of a recent tension between branching fractions for $B_{(s)} \to D_{(s)}^{(*)}M$ ($M = \pi$, K) decays in the QCD factorization approach and relevant experimental results, phenomenological constraints on complex-valued Wilson coefficients are discussed. Analyzed observables contain direct *CP* asymmetry (A_{CP}) in $B^- \to D^0\pi^-$ decays and γ/ϕ_3, one of the angles in the unitarity triangle, combined with others from τ_{B^+}/τ_{B_d}, $\Delta\Gamma_q/\Gamma_q$, and $A_{\rm SL}^q(q = d, s)$. We constrain the complex Wilson coefficients at 1σ and 2σ levels under color-singlet and color-rearranged scenarios. These constraints yield correlated predictions for $\Delta\Gamma_d/\Gamma_d$, $A_{\rm SL}^d$, and A_{CP}.

DOI: 10.1103/zhg4-zx7w

I. INTRODUCTION

Measurement of B-meson decays enables us to test various aspects of the standard model (SM), and possibly search for new physics (NP) contributions. Among a number of decay modes, nonleptonic channels require a dedicated theoretical discussion and can be compared with recent precision data in flavor factories. A theoretical framework to analyze, e.g., $B_d \to D^-K^+$ and $B_s \to D_s^-\pi^+$ is given by the QCD factorization (QCDF) approach [1], where the NP contributions can be incorporated in its short-distance parts. The analysis within the SM has been performed [2] at the next-to-next-to leading order (NNLO) in QCD corrections.

Recently, a significant tension between the branching ratios for color-allowed channels in the QCDF approach and the experimental results was pointed out in Ref. [3]: It has been claimed that power-suppressed corrections are not sufficiently large to explain the data.[1] Another work [5] discussed corrections from quasielastic rescattering [6–9], one formulation for representing final-state interactions (FSIs), revealing that branching ratios are not simultaneously accommodated within the SM. In light of the status, NP is considered a potential candidate to resolve the discrepancy [3,5,10–15]. Moreover, it is worth noting that the constraints on such NP scenarios can also be complemented by high-energy collider observables, particularly through top quark measurements and new scalar searches [16,17].

The explanation based on NP to the $B_{(s)} \to D_{(s)}^{(*)}M$ puzzle, where M represents a meson, is supposed to confront phenomenological constraints from processes related to $b \to c\bar{u}q(q = d, s)$ transitions. Specifically, B-meson lifetimes include such contributions, for which recent analyses in the SM were performed in Refs. [18–20] (See Refs. [13,21] for discussions including NP contributions). In practice, for a ratio of the lifetimes, the theoretical precision is more controlled, which would play a suitable role in constraining the NP scenarios. Furthermore, $\Delta\Gamma_q$ (see Ref. [22] for new physics study) and $A_{\rm SL}^q$ in B_q^0-$\bar{B}_q^0(q = d, s)$ mixing (see Ref. [23] for the SM analysis, and recent result in Ref. [24] at NNLO) can be also used to constrain the $b\bar{q} \to c\bar{u}$ transition and its *CP* conjugate. For this process, future precise measurement is expected in the upgrade of the LHCb [25,26], especially for $q = d$. The analyses beyond the SM including those types of the observables are carried out in Refs. [13,15] and with FSIs in Ref. [14].

Another observable sensitive to $b \to c\bar{u}q(q = d, s)$ transitions is given by γ or ϕ_3, one of the angles in the unitarity triangle (see Ref. [27] for a previous work, and Ref. [28] for

*Contact author: guoxn24@mails.jlu.edu.cn
†Contact author: panuluh@usd.ac.id
‡Contact author: umeeda@jlu.edu.cn
§Contact author: zhujl25@mails.jlu.edu.cn

[1]A recent work [4] based on light-cone sum rules discussed a possibility that particular nonfactorizable contributions lead to sizable shift, albeit large theoretical uncertainties.

Published by the American Physical Society under the terms of the Creative Commons Attribution 4.0 International license. Further distribution of this work must maintain attribution to the author(s) and the published article's title, journal citation, and DOI. Funded by SCOAP³.

an updated analysis). In light of the $B_{(s)} \to D^{(*)}_{(s)} M$ puzzle, the analysis for NP was carried out in Ref. [12] for $\bar{B}_s \to D_s^+ K^-$ and $\bar{B}_s^0 \to D_s^- K^+$ channels, based on the methodology [29] proposed primarily for the SM. In addition to Ref. [29], methods discussed by Gronau-London-Wyler (GLW) [30,31] and Atwood-Dunietz-Soni (ADS) [32,33] also provide possible channels to constrain γ/ϕ_3.

In the presence of NP contributions in $b \to c\bar{u}q$ transitions, additional CP phases possibly give direct CP asymmetries in tree-level $B \to DM$ decays.[2] Such CP violating observables from NP have been discussed for $B_s \to D_s^- K^+$ and $B_s \to D_s^+ K^-$ in Refs. [12,34]. Recently, a first measurement has been carried out in the LHCb experiment [35] for decay-time-integrated CP asymmetry in $B_s \to D_s^- \pi^+$ decays (see Ref. [36] for theory discussions in this channel). Furthermore, direct CP asymmetry for $B^- \to D^0 \pi^-$ was measured in the Belle [37–39] and LHCb [40] experiments, although the mentioned CP violating observables are both consistent with zero as expected in the SM.

In this work, the phenomenological analysis including the NP contributions in Wilson coefficients for current-current operators is carried out. From the perspective of the CP violating observables, complex-valued Wilson coefficients from NP are considered. In particular, γ/ϕ_3 and direct CP asymmetry in $B^- \to D^0 \pi^-$ decays are added to the set of the analyzed observables, which consist of the branching ratio for $B_{(s)} \to D^{(*)}_{(s)} M$ decay, the lifetime ratio (τ_{B^+}/τ_{B_d}), the width difference normalized by the total width $(\Delta\Gamma_q/\Gamma_{B_q})$, and semileptonic CP asymmetry $(A_{\rm SL}^q)$.

This paper is organized as follows: In Sec. II, we establish the theoretical foundation by formulating the effective Hamiltonian for $b \to c\bar{u}q$ transitions and addressing the relevant experimental constraints. Section III explores the implications of NP for the extraction of the unitarity triangle angle γ/ϕ_3 through GLW observables. The focus then shifts in Sec. IV to a detailed investigation of direct CP asymmetries and branching fractions within this framework. Quantitative evaluations, including phenomenological constraints on the NP Wilson coefficients and resulting predictions in light of future measurements are performed in Sec. V. Finally, we summarize our core findings and provide concluding remarks in Sec. VI.

II. EFFECTIVE HAMILTONIAN AND $\Delta B = 0$, 2 OBSERVABLES

To analyze the $\Delta B = 0$ and $\Delta B = 2$ observables, we start by defining the relevant effective Hamiltonian for the underlying $\Delta B = 1$ transitions. In our framework, we consider the nonleptonic decays $b \to c\bar{u}q$ (with $q = d, s$). Since these are charged-current transitions, penguin operators are absent. Assuming further that NP effects preserve the SM chirality and do not introduce new operator structures (such as scalar or tensor currents), but only modify the Wilson coefficients C_1^q and C_2^q, the weak effective Hamiltonian is expressed as

$$\mathcal{H}_{\rm eff}^{\Delta B=1} = \frac{G_F}{\sqrt{2}} V_{cb} V_{uq}^* [C_1^q(\mu)\mathcal{Q}_1^q + C_2^q(\mu)\mathcal{Q}_2^q] + \text{H.c.}, \quad (1)$$

where G_F is the Fermi constant and V_{ij} denotes the CKM matrix elements. The current-current four-quark operators $\mathcal{Q}_{1,2}^q$ are defined in the specific basis as

$$\mathcal{Q}_1^q = (\bar{c}^\alpha b^\beta)_{\text{V-A}} (\bar{q}^\beta u^\alpha)_{\text{V-A}}, \quad \mathcal{Q}_2^q = (\bar{c}^\alpha b^\alpha)_{\text{V-A}} (\bar{q}^\beta u^\beta)_{\text{V-A}}. \quad (2)$$

Here, α and β are color indices with implicit summation. The subscript $(\ldots)_{\text{V-A}}$ corresponds to the left-handed chiral current $\gamma^\mu(1-\gamma_5)$. The short-distance physics is encapsulated in the Wilson coefficients $C_i^q(\mu)$. Under our assumption, the total coefficients are given by the sum of the SM and NP contributions:

$$C_i^q(M_W) = C_i^{\rm SM}(M_W) + C_i^{q,\rm NP}(M_W), \quad (i = 1,2). \quad (3)$$

In our analysis, the NP contributions to the $b \to c\bar{u}d$ and $b \to c\bar{u}s$ transitions are treated as independent parameters. For the sake of brevity, we will hereafter suppress the flavor superscript q on the coefficients C_i^q, unless an explicit distinction is required. The values of these coefficients at the low-energy scale $\mu \sim m_b$ are obtained by evolving them from the electroweak scale M_W via the renormalization group equations (RGEs) [41]. For the SM predictions of the observables discussed in the following sections, we adopt values from the recent publications which incorporate contributions from tree-level as well as penguin and other loop diagrams. In contrast, the NP corrections to these observables are calculated assuming modifications solely to Wilson coefficients at the leading order (LO), where the detail is given later. The Hamiltonian in Eq. (1) serves as the fundamental input for determining the observables discussed in the following sections.

A. Lifetime ratio

In this section, we analyze the lifetime ratio τ_{B^+}/τ_{B^0}. Theoretically, the deviation of the lifetime ratio of heavy hadrons containing a heavy quark Q from unity arises primarily from spectator effects, such as weak annihilation and Pauli interference. Combining these contributions, the lifetime ratio can be expressed as

[2]Within the SM, amplitudes of tree-level $B \to DM$ decays have a common Cabibbo-Kobayashi-Maskawa (CKM) factor, $V_{cb}V_{uq}^*$, and have no interfering weak phases, leading to vanishing CP asymmetries. Hence, measurement of direct CP violation for those channels is regarded as a signal of NP.

$$\frac{\tau_{B^+}}{\tau_{B^0}} = \frac{\Gamma_{B^0}}{\Gamma_{B^+}} = \frac{\Gamma_{\rm dec} + \Gamma_{\rm ann}(B^0) + \Gamma_{\rm semi}}{\Gamma_{\rm dec} + \Gamma_{\rm int}(B^+) + \Gamma_{\rm semi}}. \tag{4}$$

Since we restrict NP effects to the $b \to c\bar{u}q$ transitions, the semileptonic decay width $\Gamma_{\rm semi}$ remains unchanged from the SM prediction. The ratio of the lifetimes is determined by the inverse ratio of the total decay widths. Including both SM and NP contributions, this is given exactly by[3]

$$\frac{\tau_{B^+}}{\tau_{B^0}} \Big/ \frac{\tau^{\rm SM}(B^+)}{\tau^{\rm SM}(B^0)} = \frac{1 + \frac{\Gamma^{\rm NP}_{\rm dec} + \Gamma^{\rm NP}_{\rm ann}(B^0)}{\Gamma^{\rm SM}(B^0)}}{1 + \frac{\Gamma^{\rm NP}_{\rm dec} + \Gamma^{\rm NP}_{\rm int}(B^+)}{\Gamma^{\rm SM}(B^+)}}, \tag{5}$$

where the SM lifetimes are defined as

$$\begin{aligned} \frac{1}{\tau^{\rm SM}(B^0)} &= \Gamma^{\rm SM}(B^0) = \Gamma^{\rm SM}_{\rm dec} + \Gamma_{\rm semi} + \Gamma^{\rm SM}_{\rm ann}(B^0), \\ \frac{1}{\tau^{\rm SM}(B^+)} &= \Gamma^{\rm SM}(B^+) = \Gamma^{\rm SM}_{\rm dec} + \Gamma_{\rm semi} + \Gamma^{\rm SM}_{\rm int}(B^+). \end{aligned} \tag{6}$$

The expressions for the decay widths ($\Gamma_{\rm dec}$, $\Gamma_{\rm ann}$, and $\Gamma_{\rm int}$) presented later are general and depend quadratically on the $\Delta B = 1$ Wilson coefficients C_1 and C_2. For the SM, LO results can be analyzed by $C_i^{\rm SM}$ while we employ the full coefficients (C_i) to include NP contributions. The formulas remain valid under this extension; one simply needs to use the full Wilson coefficients containing both SM and NP contributions. Specifically, to explicitly extract the NP contributions introduced in Eq. (5), we define them as the difference between the decay widths evaluated with the full Wilson coefficients and those evaluated with purely SM coefficients as was considered in Ref. [14]. For instance, the spectator-independent NP decay width reads

$$\Gamma^{\rm NP}_{\rm dec} = \Gamma_{\rm dec}(C_1, C_2) - \Gamma_{\rm dec}(C_1^{\rm SM}, C_2^{\rm SM}). \tag{7}$$

Similar relations hold for the spectator-dependent annihilation and Pauli interference terms, $\Gamma^{\rm NP}_{\rm ann}$ and $\Gamma^{\rm NP}_{\rm int}$. Equation (7) is used to analyze the NP contributions in Eq. (5), while the recent theoretical value [20] is adopted for $\tau^{\rm SM}(B^{+,0})$ [or equivalently $\Gamma^{\rm SM}(B^{+,0})$].

The spectator-independent decay width $\Gamma_{\rm dec}$ for $b \to c\bar{u}q$ ($q = d,\, s$) is given by [18]

$$\begin{aligned} \Gamma_{\rm dec} = \frac{G_F^2 m_Q^5}{192\pi^3}\xi \Bigg\{ & (N_c|C_1|^2 + N_c|C_2|^2 + 2{\rm Re}(C_1^* C_2)) \\ & \times \left[((1-x^2)(1-8x+x^2) - 12x^2 \ln x)\left(1 - \frac{\mu_\pi^2 - \mu_G^2}{2m_Q^2}\right) - 2(1-x)^4 \frac{\mu_G^2}{m_Q^2} \right] - 16{\rm Re}(C_1^* C_2)(1-x)^3 \frac{\mu_G^2}{m_Q^2} \Bigg\}, \end{aligned} \tag{8}$$

where the CKM factor ξ is defined as $|V_{cb}|^2|V_{uq}|^2$ for the corresponding $b \to c\bar{u}q$ transition, and $\mu^2_{\pi,G}$ represents a matrix element of a power-suppressed operator. We note that our convention for $C_{1,2}$ is interchanged relative to Ref. [18]. Additionally, all terms involving products of Wilson coefficients are generalized to $|C_i|^2$ and ${\rm Re}(C_i^* C_j)$. As to the spectator dependent effects, the neutral meson B^0 receives contributions from weak annihilation, whereas the charged meson B^+ is affected only by Pauli interference. In the $b \to c\bar{u}d$ transition, the expressions read [18]

$$\begin{aligned} \Gamma_{\rm ann}(B^0) = & -\frac{G_F^2 m_b^2}{\pi}|V_{cb}V_{ud}|^2 |\psi^B_{b\bar{q}}(0)|^2 (1-x)^2 \\ & \times \Bigg\{ \left(\frac{1}{N_c}|C_2|^2 + 2{\rm Re}(C_1^* C_2) + N_c|C_1|^2\right) \Bigg[\left(1 + \frac{x}{2}\right) B_1 - (1+2x) B_2 \\ & + \left(\frac{1+x+x^2}{1-x}\rho_3^d + \frac{6x^2}{1-x}\rho_4^d - \frac{1}{2}\left(1+\frac{x}{2}\right)\rho_5^d - \frac{1}{2}(1+2x)\rho_6^d \right)\left(\frac{m_B^2}{m_b^2} - 1\right) \Bigg] \\ & + 2|C_2|^2 \Bigg[\left(1+\frac{x}{2}\right)\epsilon_1 - (1+2x)\epsilon_2 + \left(\frac{1+x+x^2}{1-x}\sigma_3^d + \frac{6x^2}{1-x}\sigma_4^d \right. \\ & \left. - \frac{1}{2}\left(1+\frac{x}{2}\right)\sigma_5^d - \frac{1}{2}(1+2x)\sigma_6^d \right)\left(\frac{m_B^2}{m_b^2} - 1\right) \Bigg] \Bigg\}, \end{aligned} \tag{9}$$

[3]For r.h.s. in Eq. (5), we do not expand it by $1/m_b$, and instead adopt Eq. (5) since it can be used to constrain parametrically large NP contributions in the later numerical analysis.

$$\Gamma_{\rm int}(B^+) = \frac{G_F^2 m_b^2}{\pi}|V_{cb}V_{ud}|^2|\psi^B_{b\bar{q}}(0)|^2(1-x)^2 \times \left\{(2N_c{\rm Re}(C_1^* C_2) + |C_1|^2 + |C_2|^2)\left[B_1 - \left(\frac{1+x}{1-x}\rho_3^u + \frac{1}{2}\rho_5^u\right)\left(\frac{m_B^2}{m_b^2} - 1\right)\right] + 6(|C_1|^2 + |C_2|^2)\left[\epsilon_1 - \left(\frac{1+x}{1-x}\sigma_3^u + \frac{1}{2}\sigma_5^u\right)\left(\frac{m_B^2}{m_b^2} - 1\right)\right]\right\}, \tag{10}$$

where m_Q denotes the heavy quark mass ($Q = b$ for B mesons), and $N_c = 3$ is the number of colors. Other relevant hadronic parameters include $d_H = 3$, the mass ratio $x = (\bar{m}_c/\bar{m}_b)^2$, the decay constant f_B entering via $|\psi^B_{b\bar{q}}(0)|^2 = \frac{1}{12}f_B^2 m_B$, and the bag parameters, B_1, ϵ_1, ρ_1 and σ_1. The strange quark contributions similar to Eqs. (9) and (10) can be obtained by the replacement of flavors.

B. B-$\bar{B}$ mixing

In the neutral B_q-$\bar{B}_q$ mixing system ($q = d, s$), the ratio of the absorptive part to the dispersive part of the mass matrix, $|\Gamma^q_{21}/M^q_{21}|$, is of the order $\mathcal{O}(m_b^2/m_t^2) \sim 10^{-3}$. Consequently, we can safely neglect terms of $\mathcal{O}(m_b^4/m_t^4)$ in the mixing observables. Based on this hierarchy, the width difference $\Delta\Gamma_q$ and the semileptonic CP asymmetry $A^q_{\rm SL}$ are given by

$$\Delta\Gamma_q = -2|M^q_{21}|{\rm Re}\left(\frac{\Gamma^q_{21}}{M^q_{21}}\right), \quad A^q_{\rm SL} \approx {\rm Im}\left(\frac{\Gamma^q_{12}}{M^q_{12}}\right) = -{\rm Im}\left(\frac{\Gamma^q_{21}}{M^q_{21}}\right), \tag{11}$$

where the off-diagonal matrix elements are expressed as [42]

$$\Gamma^q_{21} = -\frac{G_F^2 m_b^2}{24\pi M_{B_q}}\left[c_1^q\langle\bar{B}_q|\mathcal{O}_1^q|B_q\rangle + c_2^q\langle\bar{B}_q|\mathcal{O}_2^q|B_q\rangle + \delta^q_{1/m}\right],$$
$$M^q_{21} = \frac{G_F^2 M_W^2 \eta_B}{(4\pi)^2(2M_{B_q})}(V_{tb}^* V_{tq})^2 S_0(x_t)\langle\bar{B}_q|\mathcal{O}_1^q|B_q\rangle, \tag{12}$$

where renormalization scales for $\Delta B = 1$ and $\Delta B = 2$ operators, not displayed explicitly for brevity, are set to a common one. η_B is the perturbative QCD correction factor, and $S_0(x_t)$ is the Inami-Lim function [43] describing the short-distance top-quark loop contribution to $\Delta B = 2$ processes, with $x_t = m_t^2/M_W^2$:

$$S_0(x) = \frac{4x - 11x^2 + x^3}{4(1-x)^2} - \frac{3x^3\ln x}{2(1-x)^3}. \tag{13}$$

The coefficients c_i^q and the $1/m_b$ correction term $\delta^q_{1/m}$ in Eq. (12) encapsulate the contributions from the charm and up quark loops in the correlator calculation [42]:

$$c_i^q = (V_{tb}^* V_{tq})^2 D_i^{uu} + 2V_{cb}^* V_{cq} V_{tb}^* V_{tq}(D_i^{uu} - D_i^{cu}) + (V_{cb}^* V_{cq})^2(D_i^{cc} + D_i^{uu} - 2D_i^{cu}),$$
$$\delta^q_{1/m} = (V_{tb}^* V_{tq})^2\delta^{uu,q}_{1/m} + 2V_{cb}^* V_{cq} V_{tb}^* V_{tq}(\delta^{uu,q}_{1/m} - \delta^{cu,q}_{1/m}) + (V_{cb}^* V_{cq})^2(\delta^{cc,q}_{1/m} + \delta^{uu,q}_{1/m} - 2\delta^{cu,q}_{1/m}). \tag{14}$$

The detailed definitions of the $\Delta B = 2$ operator basis, along with their corresponding hadronic matrix elements, are listed in the Appendix.

To study NP effects, we incorporate the modified Wilson coefficients C_1 and C_2 (from the $\Delta B = 1$ sector) into the calculation of Γ^q_{21}. The mass difference M^q_{21} remains dominated by the SM top-quark loops and is unaffected by the NP considered here. Consequently, the constraints from B_q-$\bar{B}_q$ mixing observables can be derived as

$$\Delta\Gamma_q|_{\rm exp} = -2|M^q_{21}|{\rm Re}\left(\frac{\Gamma^q_{21,\rm SM} + \Gamma^q_{21,\rm NP}}{M^q_{21}}\right) = \Delta\Gamma_{q,\rm SM} - 2|M^q_{21}|{\rm Re}\left(\frac{\Gamma^q_{21,\rm NP}}{M^q_{21}}\right),$$
$$A^q_{\rm SL}|_{\rm exp} = -{\rm Im}\left(\frac{\Gamma^q_{21,\rm SM} + \Gamma^q_{21,\rm NP}}{M^q_{21}}\right) = A^q_{\rm SL,SM} - {\rm Im}\left(\frac{\Gamma^q_{21,\rm NP}}{M^q_{21}}\right), \tag{15}$$

where $\Gamma^q_{21,\rm SM}$ and $\Gamma^q_{21,\rm NP}$ are defined in a way similar to Eq. (7), i.e., by evaluating the off-diagonal decay matrix element with purely SM coefficients and by taking the difference between the full result and the SM one, respectively [$\Gamma^q_{21,\rm NP} = \Gamma^q_{21}(C_1, C_2) - \Gamma^q_{21}(C_1^{\rm SM}, C_2^{\rm SM})$]. For $\Gamma_{q,\rm SM}$ and $A^q_{\rm SL,SM}$, the recent precise theoretical values [23] are used in the later numerical analysis.

III. UNITARITY TRIANGLE AND NEW PHYSICS

A. Parametrization of tree-level decays

Two-body hadronic B-meson decays are classified according to their flavor topology into color-allowed tree (T), color-suppressed tree (C), exchange (E), and annihilation (A) diagrams. Among these, the T diagram is the only component reliably calculable using the QCDF approach. For instance, the factorization amplitude for the process $\bar{B}_s^0 \to D_s^+ K^-$ is given by

$$T(\bar{B}_s^0 \to D_s^+ K^-) = \frac{G_F}{\sqrt{2}} V_{us}^* V_{cb} f_{K^-} F_0^{B_s \to D_s}(m_{K^-}^2)(m_{B_s}^2 - m_{D_s}^2) a_1(D_s K), \tag{16}$$

where G_F is the Fermi constant, V_{us} and V_{cb} are the relevant CKM matrix elements, f_{K^-} is the decay constant, and $F_0^{B_s \to D_s}$ is the transition form factor evaluated at $q^2 = m_{K^-}^2$.

To account for E diagram, an effective parameter a_1^{eff} is often defined to replace the Wilson coefficient combination,

$$a_1^{\text{eff}}(D_s K) = a_1(D_s K)\left(1 + \frac{E_{D_s K}}{T_{D_s K}}\right). \tag{17}$$

A similar parametric form that absorbs the hadronic complexity into the effective coefficient is used as a notation for amplitudes proportional to $T + C$. In the following sections, we will discuss the evaluation of these hadronic ratios.

B. New physics phase

Our analysis of NP effects in the unitarity triangle determination relies on modifying the effective parameter a_1 governing the nonleptonic tree-level decays. It is crucial to distinguish the quark-level transitions $\bar{b} \to \bar{c}u\bar{q}$ (where $q = d, s$) and their CP-conjugate counterparts $b \to c\bar{u}q$.

For the $b \to c\bar{u}q$ transitions (e.g., in B^- or $\bar{B}^0$ decays), the NP Wilson coefficients enter directly without complex conjugation for the convention in Eq. (1). Thus, we generalize the parameter a_1 as

$$a_1(b \to c) = a_1^{\text{SM}} + C_2^{\text{NP}} + \frac{C_1^{\text{NP}}}{3}, \tag{18}$$

where C_1^{NP} and C_2^{NP} are the complex coefficients of the operators $\mathcal{Q}_1^q$ and $\mathcal{Q}_2^q$ in the NP effective Hamiltonian respectively. In contrast, for the CP-conjugate transitions $\bar{b} \to \bar{c}u\bar{q}$ (e.g., in B^+ or B^0 decays), the Wilson coefficients must be complex conjugated ($C_i^{\text{NP}} \to C_i^{\text{NP}*}$).

To parametrize this effect, we define a magnitude modification and a new weak phase ρ based on the unconjugated b transition

$$a_1(b \to c) = a_1^{\text{SM}}\left(1 + \frac{C_2^{\text{NP}} + C_1^{\text{NP}}/3}{a_1^{\text{SM}}}\right) \equiv a_1^{\text{SM}}|1 + \eta|e^{i\rho}, \tag{19}$$

where we set a_1^{SM} to its absolute value (since the strong phase of this quantity is rather tiny [1,2,11] in the context of our present work), and the auxiliary parameters are defined as

$$\eta = \frac{C_2^{\text{NP}} + C_1^{\text{NP}}/3}{a_1^{\text{SM}}}, \qquad \rho = \text{Arg}(1 + \eta). \tag{20}$$

Consequently, the effective parameter for the conjugate $\bar{b} \to \bar{c}$ transitions is given by $a_1^{\text{SM}}|1 + \eta|e^{-i\rho}$.

C. Modification of observables under new physics

To evaluate the impact of the NP phase ρ defined in the previous section, we examine the ratio of the suppressed to favored amplitudes. In the SM, this ratio is parametrized as

$$\frac{A_{\text{sup}}}{A_{\text{fav}}} = r_B e^{i(\delta_B \pm \gamma)}, \tag{21}$$

where r_B is the magnitude ratio, δ_B is the strong phase difference, and the $\pm$ sign corresponds to $B^{\mp}$ decays.

We assume that the NP contribution enters only through the effective parameter a_1 in the Cabibbo-favored process ($b \to c$), as defined in Eq. (18), without altering Cabibbo-suppressed decay ($b \to u$). Consequently, the amplitudes for the process $B^+ \to DK^+$ are modified as follows:

$$A(B^+ \to D^0 K^+) = |A_{\text{sup}}^{\text{SM}}|e^{i\gamma}e^{i\delta}, \tag{22}$$

$$A(B^+ \to \bar{D}^0 K^+) = |A_{\text{fav}}^{\text{SM}}|e^{i\bar{\delta}}|1 + \eta|e^{-i\rho}. \tag{23}$$

Note that Eq. (23) provides a compact parametrization for the amplitude, and remains fundamentally equivalent to the factorization framework used later for evaluating the branching fractions. In Sec. IV B, a model-independent treatment is further adopted to extract the color-suppressed hadronic contributions from experimental data to avoid large theoretical uncertainties. Substituting these into the ratio, we obtain the effective amplitude ratio

$$\left.\frac{A_{\text{sup}}}{A_{\text{fav}}}\right|_{\text{eff}} = \frac{A_{\text{sup}}^{\text{SM}}}{A_{\text{fav}}^{\text{SM}}(1 + \eta^*)} = \frac{r_B}{|1 + \eta|} e^{i(\delta_B + \gamma + \rho)}, \tag{24}$$

where $r_B = |A_{\text{sup}}^{\text{SM}}|/|A_{\text{fav}}^{\text{SM}}|$ and $\delta_B = \delta - \bar{\delta}$. Crucially, we observe that the functional form of the ratio remains

invariant. The NP effects can be absorbed by redefining the experimental parameters:

$$r_B^{\rm exp} = \frac{r_B}{|1+\eta|}, \qquad \gamma^{\rm exp} = \gamma_i + \rho, \tag{25}$$

where $i =$ indirect or direct, and specific values of γ_i are introduced later. The GLW observables are experimentally defined via the ratios of partial decay widths involving CP eigenstates $D_{CP\pm}$ [44]:

$$R_{CP\pm} = \frac{\Gamma(B^- \to D_{CP\pm}K^-) + \Gamma(B^+ \to D_{CP\pm}K^+)}{\Gamma(B^- \to D^0K^-) + \Gamma(B^+ \to \bar{D}^0K^+)}, \tag{26}$$

$$A_{CP\pm} = \frac{\Gamma(B^- \to D_{CP\pm}K^-) - \Gamma(B^+ \to D_{CP\pm}K^+)}{\Gamma(B^- \to D_{CP\pm}K^-) + \Gamma(B^+ \to D_{CP\pm}K^+)}. \tag{27}$$

Therefore, the standard expressions for the GLW observables $R_{CP\pm}$ and $A_{CP\pm}$ remain valid under the replacements $r_B \to r_B^{\rm exp}$ and $\gamma \to \gamma^{\rm exp}$:

$$R_{CP\pm} = 1 + (r_B^{\rm exp})^2 \pm 2r_B^{\rm exp}\cos\delta_B\cos\gamma^{\rm exp}, \tag{28}$$

$$A_{CP\pm} = \frac{\pm 2r_B^{\rm exp}\sin\delta_B\sin\gamma^{\rm exp}}{R_{CP\pm}}. \tag{29}$$

This confirms that a NP phase in the tree-level Wilson coefficient manifests simply as a shift in the extracted CKM angle γ. In the later numerical analysis, the second relation in Eq. (25) is used to constrain the Wilson coefficients.

IV. DIRECT CP AND BRANCHING RATIO

A. Direct CP violation

Having established the phenomenological impact of NP on the GLW observables, we now turn to the theoretical calculation of the underlying partial widths and direct CP asymmetries within the SM. Based on the underlying mechanisms, CP violation is usually classified into three types: direct violation, indirect violation, and CP violation arising from the interference between decay and mixing. In charged B meson decays, there is no mixing phenomenon, and direct CP violation is the only observable effect. Specifically, the corresponding asymmetry is defined as

$$A_{CP}(B^+ \to f^+) \equiv \frac{\Gamma(B^- \to f^-) - \Gamma(B^+ \to f^+)}{\Gamma(B^- \to f^-) + \Gamma(B^+ \to f^+)}. \tag{30}$$

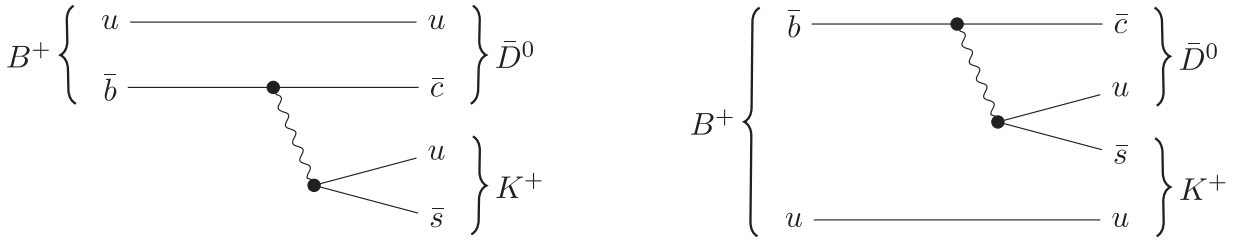
It is important to emphasize that the equation above represents the generic definition of direct CP asymmetry for a specific final state f. This should be distinguished from the GLW observable $A_{CP\pm}$ discussed in the previous section, which specifically refers to the asymmetry involving CP eigenstate modes ($D_{CP\pm}$) and involves a different normalization factor (the denominator is normalized to the flavor-specific modes). The partial width for a specific decay, for instance $B^- \to D^0\pi^-$, can be calculated within the framework of perturbative QCD (PQCD). It is proportional to the squared magnitude of the decay amplitude [45],

$$\Gamma(B^- \to D^0\pi^-) = \frac{1}{128\pi}G_F^2|V_{cb}|^2|V_{ud}|^2\frac{m_B^3}{r}|A_{D^0\pi^-}|^2, \tag{31}$$

with r defined in Eq. (C4). In the PQCD approach, the total decay amplitude $A_{D^0\pi^-}$ is systematically decomposed into contributions from different Feynman diagram topologies [45]:

$$A_{D^0\pi^-} = f_\pi\xi_{\rm ext} + f_D\xi_{\rm int} + \mathcal{M}_{\rm ext} + \mathcal{M}_{\rm int}. \tag{32}$$

Here, $\xi_{\rm ext}$ and $\xi_{\rm int}$ denote the factorizable external W-emission (color-allowed) and internal W-emission (color-suppressed) contributions, respectively, while $\mathcal{M}_{\rm ext}$ and $\mathcal{M}_{\rm int}$ denote the corresponding nonfactorizable contributions. For this charged mode, the W-exchange topology does not enter the class-III amplitude. The explicit PQCD expressions for these building blocks, including the hard kernels, evolution factors and meson distribution amplitudes, are collected in Appendix C.



(a) T diagram (b) C diagram

FIG. 1. Topological diagrams contributing to $B^+ \to \bar{D}^0K^+$.

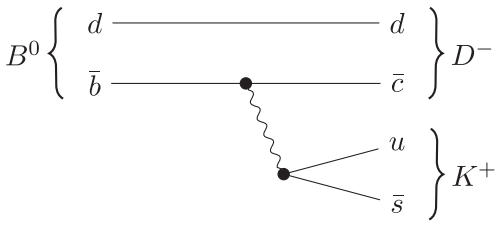


FIG. 2. The reference decay channel $B^0 \to D^- K^+$, which proceeds via the T diagram.

B. Branching ratio

For a general two-body decay $B \to M_1 M_2$, the branching ratio is given by

$$\mathcal{B}(B \to M_1 M_2) = \frac{\Gamma(B \to M_1 M_2)}{\Gamma_{\text{tot}}} = \frac{|\mathbf{p}|}{8\pi m_B^2} |\mathcal{M}|^2 \tau_B, \quad (33)$$

where τ_B is the lifetime of the B meson. $|\mathbf{p}|$ denotes the magnitude of the 3-momentum of the final state particles in the rest frame of the decaying meson, defined as

$$|\mathbf{p}| = \frac{\Phi(m_B, m_{M_1}, m_{M_2})}{2m_B},$$
$$\text{with} \quad \Phi(x,y,z) \equiv \sqrt{[x^2 - (y+z)^2][x^2 - (y-z)^2]}. \quad (34)$$

Here, $\mathcal{M}$ represents the total amplitude, which is generally a linear combination of different topological amplitudes, such as T, C, E, and A diagrams. For the specific decay $B^+ \to \bar{D}^0 K^+$, the amplitude receives contributions from both T and C topologies, as illustrated in Fig. 1. While the T diagram can be reliably calculated using, e.g., the QCDF approach, the C diagram suffers from large hadronic uncertainties and cannot be calculated directly with high precision.

To evaluate the total amplitude $\mathcal{M}(B^+ \to \bar{D}^0 K^+) = T + C$, we adopt a phenomenological approach inspired by the method proposed in [12] (originally for $T + E$ topologies). We utilize $SU(2)$ isospin symmetry to relate the process of interest to the reference decay $B^0 \to D^- K^+$, which is dominated by the color-allowed tree diagram (see Fig. 2).

Using the experimental branching ratios and the theoretical expression for the T diagram, we can extract the contribution of the C diagram. The ratio of the squared amplitudes is related to the observables by

$$\left|\frac{T_{\bar{D}^0 K^+}}{T_{D^- K^+}}\right|^2 \left|1 + \frac{C_{\bar{D}^0 K^+}}{T_{\bar{D}^0 K^+}}\right|^2 = \frac{\tau_{B^0}}{\tau_{B^+}} \left(\frac{m_{B^+}}{m_{B^0}}\right)^3 \left[\frac{\Phi(m_{B^0}, m_{D^-}, m_{K^+})}{\Phi(m_{B^+}, m_{\bar{D}^0}, m_{K^+})}\right] \left[\frac{\mathcal{B}(B^+ \to \bar{D}^0 K^+)}{\mathcal{B}(B^0 \to D^- K^+)}\right]. \quad (35)$$

The theoretical ratio of the T amplitudes is given by factorization as

$$\left|\frac{T_{\bar{D}^0 K^+}}{T_{D^- K^+}}\right| = \left[\frac{F_0^{B^+ \to \bar{D}^0}(m_{K^+}^2)}{F_0^{B^0 \to D^-}(m_{K^+}^2)}\right] \left[\frac{m_{B^+}^2 - m_{\bar{D}^0}^2}{m_{B^0}^2 - m_{D^-}^2}\right] \left|\frac{a_1(\bar{D}^0 K^+)}{a_1(D^- K^+)}\right|. \quad (36)$$

Finally, the total amplitude for the $B^+ \to \bar{D}^0 K^+$ decay is evaluated as

$$|\mathcal{M}(B^+ \to \bar{D}^0 K^+)|^2 = |T_{\bar{D}^0 K^+}|^2 \left|1 + \frac{C_{\bar{D}^0 K^+}}{T_{\bar{D}^0 K^+}}\right|^2. \quad (37)$$

With the total amplitude determined, we can subsequently introduce NP corrections in T diagrams. $|1 + C/T|^2$ in Eq. (37) is model independently extracted from the data by using Eqs. (35) and (36).

V. NUMERICAL RESULTS

A. Experimental inputs and SM predictions

For the γ inputs, we consider the following three values:

$$\gamma_{\text{indirect}} = 73.27°, \quad (38)$$
$$\gamma_{\text{direct}} = (66.4^{+2.7}_{-2.8})°, \quad (39)$$
$$\gamma_{\text{CKMfitter}} = 66.33°. \quad (40)$$

In Eq. (38), the indirect central value is obtained by using the unitarity relation $\alpha + \beta + \gamma = 180°$ with α and β from HFLAV [46,47]. Because this indirect determination is almost free from tree-level NP effects in $b \to c\bar{u}q$ transitions, it is used as the primary input in our subsequent numerical analysis. As for Eq. (39), it is given by direct measurement [46,47]. For Eq. (40), $\gamma_{\text{CKMfitter}}$ is obtained from the definition $\gamma = -\arg(V_{ud} V_{ub}^* / V_{cd} V_{cb}^*)$ using the Wolfenstein parameters from CKMfitter [48,49].

Unlike the indirect value, γ_{direct} is sensitive to NP contributions, while $\gamma_{\text{CKMfitter}}$ is also affected to a lesser extent. Direct measurements of γ and the branching ratios used in our analysis are summarized in Tables I and II, respectively.

For the lifetime ratio $\tau(B^+)/\tau(B^0)$, the comparison between the experimental world average [46] and the SM prediction [20] yields

$$\left(\frac{\tau_{B^+}}{\tau_{B^0}}\right)_{\text{Exp}} = 1.076 \pm 0.004,$$
$$\left(\frac{\tau_{B^+}}{\tau_{B^0}}\right)_{\text{SM}} = 1.081 \pm 0.016. \quad (41)$$

Regarding the neutral meson mixing observables, the experimental values [46] for the width difference $\Delta\Gamma_q/\Gamma_{B_q^0}$ and the semileptonic asymmetry A_{SL}^q (with $q = d, s$) are

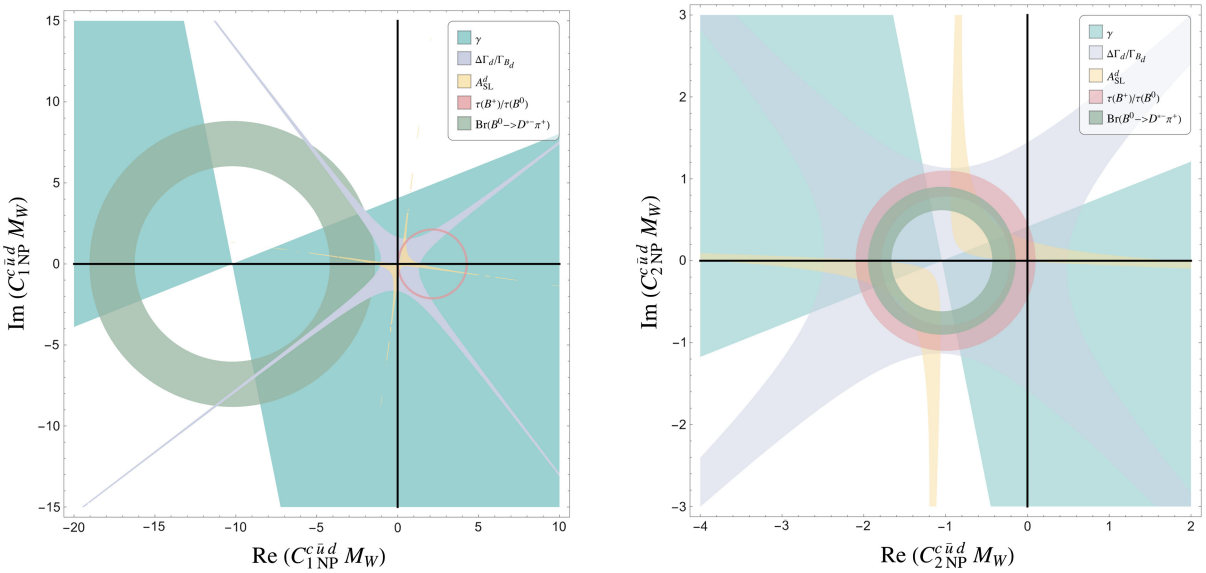


FIG. 3. Combined constraints on the NP Wilson coefficient $C^{c\bar{u}d}_{1,\mathrm{NP}}(M_W)$ and $C^{c\bar{u}d}_{2,\mathrm{NP}}(M_W)$ from various flavor observables for $B_d \to D^{*-}\pi^+$ at 1σ level. The different colored regions represent the following constraints: the cyan wedge for the CKM angle γ; the red and green bands for the lifetime ratio $\tau(B^+)/\tau(B^0)$ and the branching ratio $\mathrm{Br}(B_d \to D^{*-}\pi^+)$, respectively; the light purple and yellow regions for the mixing observables $\Delta\Gamma_d/\Gamma_{B_d}$ and A^d_{SL}.

$$\left.\frac{\Delta\Gamma_d}{\Gamma_{B^0_d}}\right|_{\mathrm{Exp}} = 0.001 \pm 0.010,$$
$$A^d_{\mathrm{SL,Exp}} = -0.0021 \pm 0.0017,$$
$$\left.\frac{\Delta\Gamma_s}{\Gamma_{B^0_s}}\right|_{\mathrm{Exp}} = 0.124 \pm 0.007,$$
$$A^s_{\mathrm{SL,Exp}} = -0.0006 \pm 0.0028. \tag{42}$$

For the future experimental projection, the uncertainties are expected to be significantly reduced at LHCb [25,26]. These projections read

$$\delta\left(\frac{\Delta\Gamma_d}{\Gamma_d}\right)_{\mathrm{future}} = 1 \times 10^{-3}, \qquad \delta(\mathcal{A}^d_{\mathrm{SL}})_{\mathrm{future}} = 2 \times 10^{-4}. \tag{43}$$

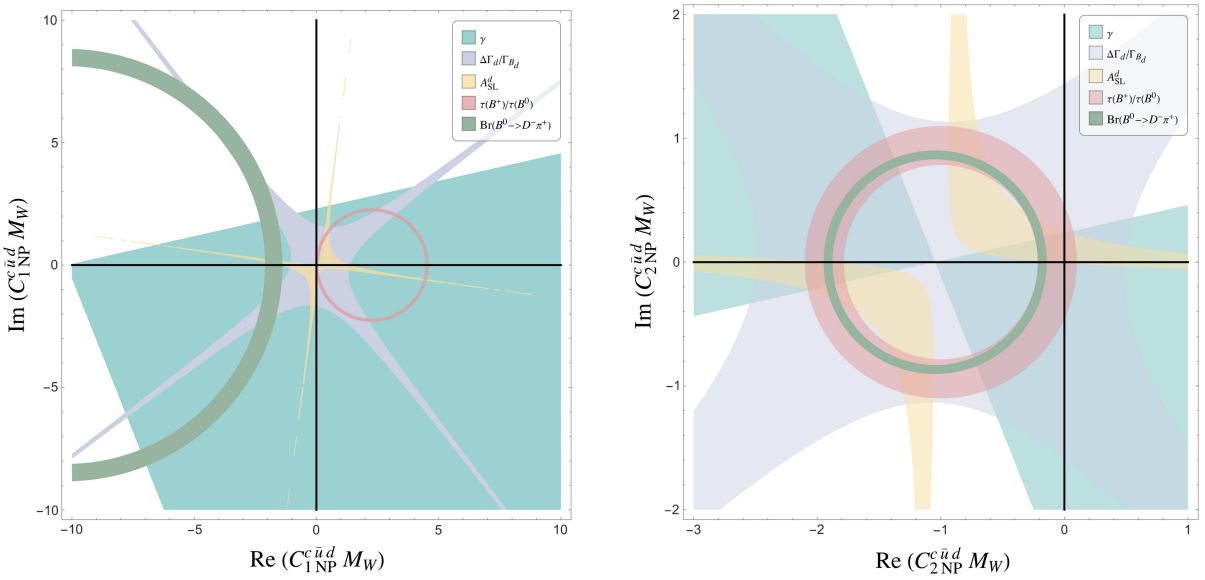


FIG. 4. Combined constraints on the NP Wilson coefficient $C^{c\bar{u}d}_{1,\mathrm{NP}}(M_W)$ and $C^{c\bar{u}d}_{2,\mathrm{NP}}(M_W)$ from various flavor observables for $B_d \to D^-\pi^+$ at 1σ level.

The corresponding SM predictions have been presented in Ref. [23]:

$$\begin{aligned}\Delta\Gamma_{d,\mathrm{SM}} &= 0.0027 \pm 0.0004\ \mathrm{ps}^{-1},\\ A^{d}_{\mathrm{SL,SM}} &= -0.00051 \pm 0.00005,\\ \Delta\Gamma_{s,\mathrm{SM}} &= 0.091 \pm 0.015\ \mathrm{ps}^{-1},\\ A^{s}_{\mathrm{SL,SM}} &= 0.000022 \pm 0.000002.\end{aligned} \tag{44}$$

In the analysis, while contributions of NP and interference between NP and the SM are evaluated at LO in QCD, the SM contributions are extracted from recent publications. The SM prediction for $\tau(B^+)/\tau(B^0)$ is taken from the NLO-QCD HQE result [20], and the SM predictions for the neutral meson mixing observables are adopted at the NLO-QCD level from Ref. [23]. For the branching-ratio constraints, the SM factorization input is taken from the NNLO QCDF result [2].

The experimental value for the CP asymmetry

$$A_{CP}(B^+ \to \bar{D}^0\pi^+) = (-3.2 \pm 3.5) \times 10^{-3} \tag{45}$$

is taken from PDG [44] based on the LHCb [40] and Belle [38,39] experiments (see also previous measurement in the Belle experiment [37]).

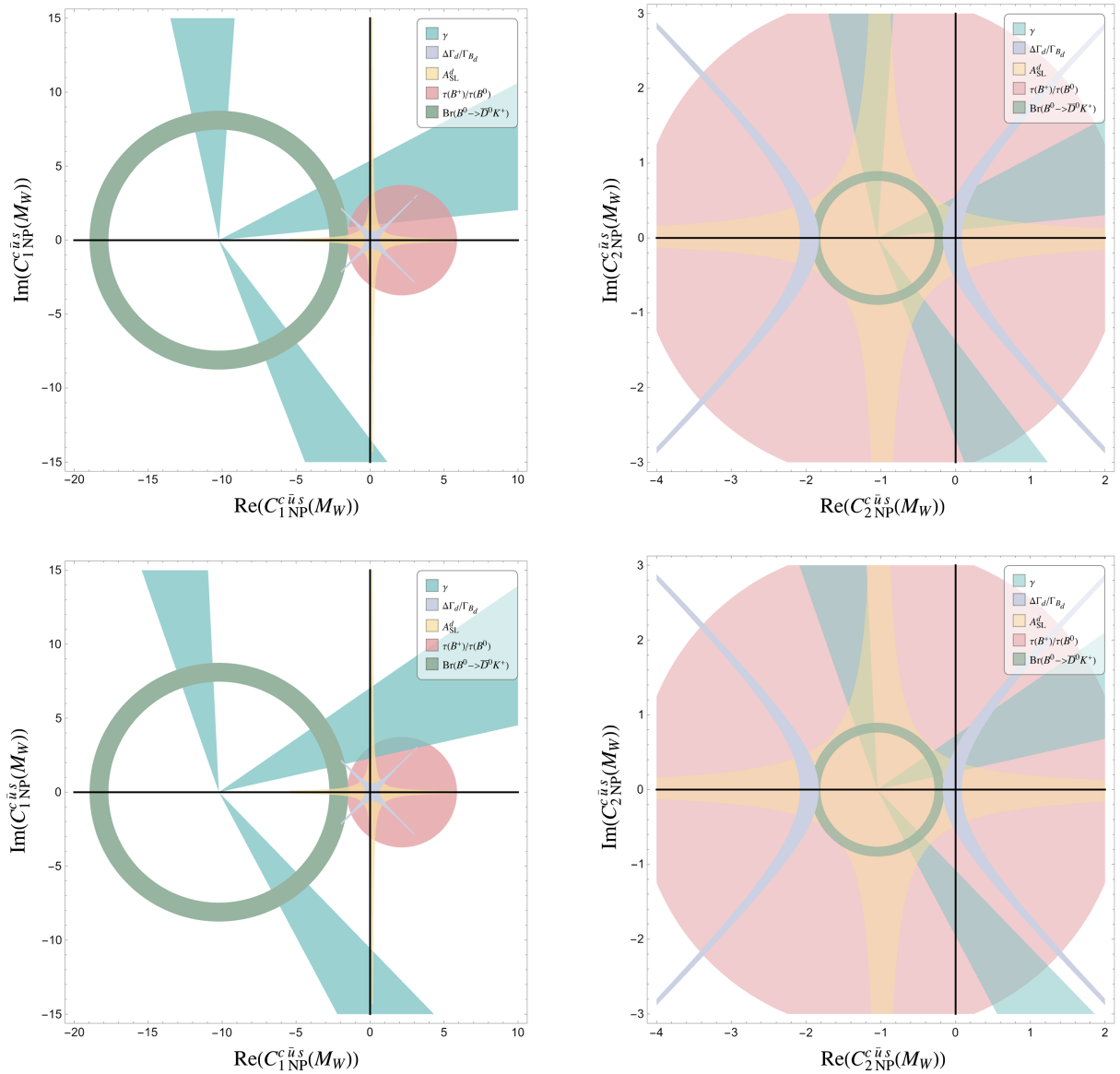


FIG. 5. Combined constraints on the NP Wilson coefficients $C^{c\bar{u}s}_{1,\mathrm{NP}}(M_W)$ and $C^{c\bar{u}s}_{2,\mathrm{NP}}(M_W)$ from various flavor observables for $B^+ \to \bar{D}^0 K^+$ at 2σ level. The upper panels are obtained using $\gamma_{\mathrm{indirect}} = 73.27°$, while the lower panels serve as a robustness check using $\gamma_{\mathrm{direct}} = 66.4°$.

B. Constraints on Wilson coefficients

In what follows, we present the 1σ and 2σ allowed regions for the NP Wilson coefficients $C_i^{\rm NP}(M_W)$ $(i=1,2)$ in the complex plane. Since $C_1^{\rm NP}$ and $C_2^{\rm NP}$ are in general complex parameters, the full parameter space is four-dimensional. In this subsection, we consider simplified two-parameter scenarios as follows:

(i) The left panels show the constraints on $C_1^{\rm NP}(M_W)$ with the boundary condition $C_2^{\rm NP}(M_W)=0$.
(ii) The right panels show the constraints on $C_2^{\rm NP}(M_W)$ with the boundary condition $C_1^{\rm NP}(M_W)=0$.

The observables are evaluated at $\mu=m_b$, and thus short-distance QCD corrections from M_W to m_b for the Wilson coefficients are considered in a relevant way. In this case, $C_1(m_b)$ and $C_2(m_b)$ are nonzero in general for both of the mentioned scenarios.

For the unitarity-triangle and branching-ratio constraints, the observables are evaluated at $\mu=\bar{m}_b(\bar{m}_b)$, where $\alpha_s=0.224$. Regarding the lifetime-ratio constraints, we use the kinetic-scheme inputs, including $m_b^{\rm kin}$ and the HQE parameters μ_π^2, μ_G^2 and ρ_D^3, consistently with their extraction from inclusive semileptonic B-decay fits [50]; the strong coupling is evaluated at $\mu=m_b^{\rm kin}/2$, giving $\alpha_s=0.281$. For the B^0-$\bar{B}^0$ mixing observables, we evaluate the relevant coefficients at the common scale $\mu_1=\mu_2=m_b^{\rm pole}$, with $\alpha_s=0.215$. The scale evolution of α_s and quark masses is performed using the RUNDEC package [51]. The detailed input values are listed in Table III.

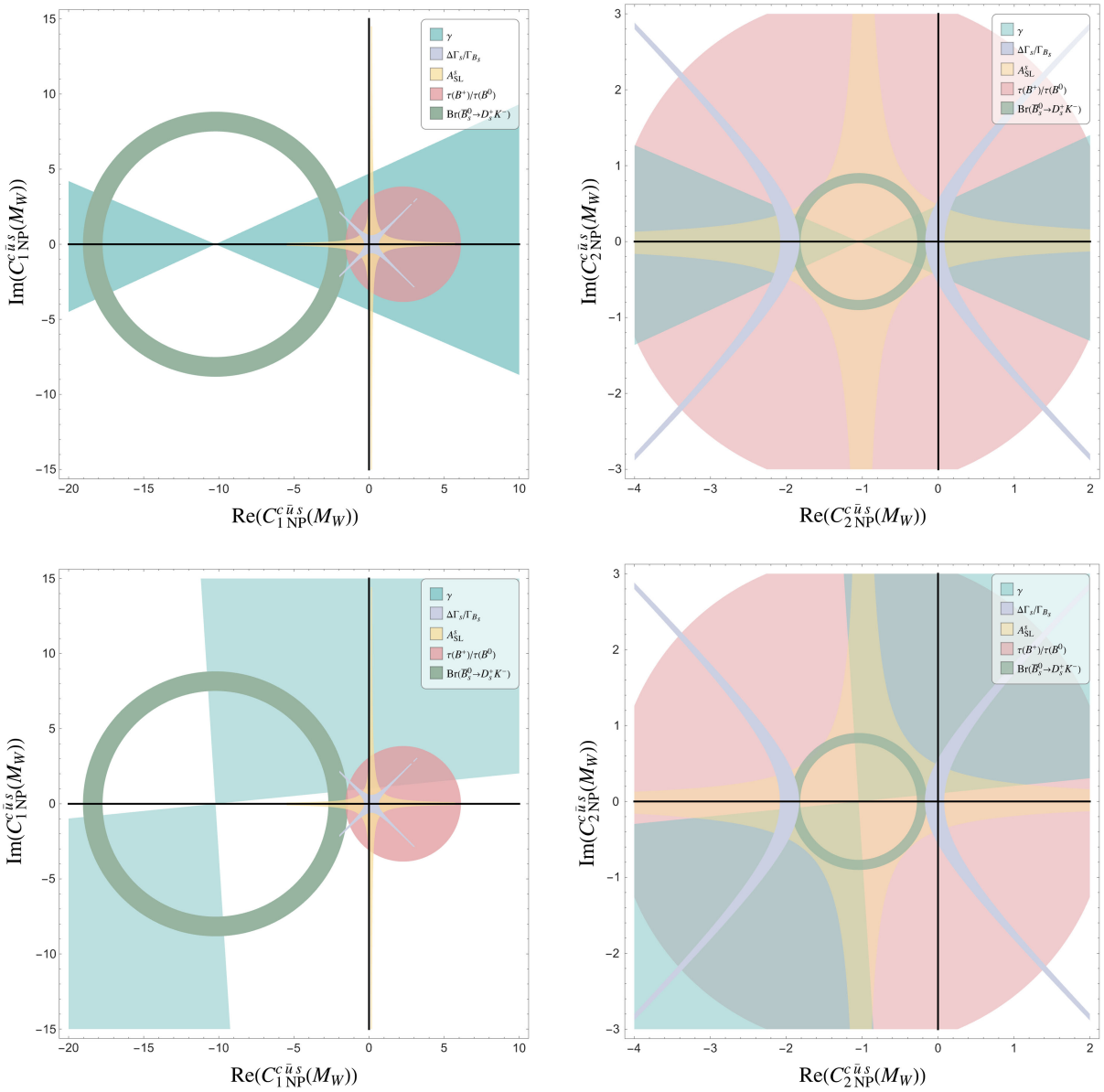


FIG. 6. Combined constraints on the NP Wilson coefficients $C_{1,\rm NP}^{c\bar{u}s}(M_W)$ and $C_{2,\rm NP}^{c\bar{u}s}(M_W)$ for $\bar{B}_s^0\to D_s^+K^-$ at the 2σ level. The upper panels correspond to the range $\gamma^{\rm exp}\in[62°,86°]$ [52], while the lower panels correspond to $\gamma^{\rm exp}\in[101°,145°]$ [53].

For constraints on the parameters, relevant observables are evaluated on a complex plane, with allowed regions of each quantity illustrated in figures, instead of performing a global χ^2 fit. The resulting allowed regions are obtained from the overlap of the individual constraints. As for the treatment of uncertainties, we combine the experimental and the SM errors in the following ways: For the neutral meson mixing, based on Eq. (15), the combined objects of $\Delta\Gamma_q|_{\rm exp} - \Delta\Gamma_q|_{\rm SM}$ and $A^q_{\rm SL}|_{\rm exp} - A^q_{\rm SL}|_{\rm SM}$ are used to constrain the NP parameters, where Gaussian 10^6 samples for both theoretical and experimental inputs are generated to evaluate the central values and uncertainties of those quantities. Regarding the lifetime ratio in Eq. (5) and the branching ratios, similar ways of combining uncertainties are implemented with the SM uncertainties from the CKM matrix elements and form factors for the latter.

To constrain possible NP effects, we use a set of independent observables from the channels $B_d \to D^{(*)-}\pi^+$ for $b \to c\bar{u}d$ and $B^+ \to \bar{D}^0 K^+$ and $\bar{B}^0_s \to D^+_s K^-$ for $b \to c\bar{u}s$. The resulting constraints are shown in the complex planes of the corresponding high-scale NP Wilson coefficients $C^{\rm NP}_i(M_W)$.

For each channel, the combined allowed region is identified as the overlap of the individual constraints. For both the $b \to c\bar{u}s$ and $b \to c\bar{u}d$ transitions, the allowed regions show tension with the SM point (the crossing point for black solid lines), in agreement with earlier observations, e.g., Ref. [3]. For the $b \to c\bar{u}d$ transition, a common overlap appears already at the 1σ level in the $C^{\rm NP}_1(M_W) = 0$ scenario, while the SM point lies outside this region; see the right panels of Figs. 3 and 4. For the $b \to c\bar{u}s$ transition, the individual 1σ constraints do not have a common overlap once the mixing observables are included, and we therefore show the viable region at the 2σ level in Figs. 5 and 6. Overall, the constraints tend to favor nonzero NP contributions, especially in the $C^{\rm NP}_1(M_W) = 0$ scenario.

The two one-operator scenarios lead to visibly different constraint patterns. As shown representatively in Fig. 5, the constraints from γ and the branching ratios are weaker in the $C^{\rm NP}_2(M_W) = 0$ scenario than in the $C^{\rm NP}_1(M_W) = 0$ scenario. This reflects the weaker sensitivity of these observables to NP contributions in the color-rearranged operator $\mathcal{Q}_1$ compared with the color-singlet operator $\mathcal{Q}_2$, due to the $1/N_c$ color suppression of the former.

We also examine the impact of the different CKM angle γ inputs. In addition to the results obtained with $\gamma_{\rm indirect} = 73.27°$, we show the constraints using $\gamma_{\rm direct} = 66.4°$ in Fig. 5 for the $B^+ \to \bar{D}^0 K^+$ channel as a representative check. The change in γ just rotates the corresponding allowed regions in the complex plane, while the overall overlap pattern remains qualitatively unchanged. As for $\gamma_{\rm CKMfitter}$, it gives results visually indistinguishable from those obtained from $\gamma_{\rm direct} = 66.4°$; hence the plots only for $\gamma_{\rm indirect}$ and $\gamma_{\rm direct}$ are displayed. We have verified that the other decay channels show similar behavior when alternative γ inputs are used.

C. B_d-$\bar{B}_d$ mixing and direct CP violation

In Fig. 7, the predicted correlation between the width difference normalized by the total width $\Delta\Gamma_d/\Gamma_d$ and the semileptonic asymmetry A^d_{SL} is shown as allowed regions for the baseline scenario $C^{\rm NP}_1(M_W) = 0$ with $C^{\rm NP}_2(M_W) \neq 0$. The green region is derived from a parameter space that satisfies three independent constraints: (i) the direct measurement of the CKM angle γ, (ii) the branching ratio of the $B_d \to D^-\pi^+$ decay, and (iii) the lifetime ratio $\tau(B^+)/\tau(B^0_d)$, simultaneously at 68% CL. For comparison, the orange region shows the prediction when the constraint from the CKM angle γ is excluded from the set of constraints. It should be noted that the orange region also lies behind the green ones in Figs. 7–9. The resulting allowed regions for $C^{\rm NP}_2(M_W)$ are then mapped onto the $(\Delta\Gamma_d/\Gamma_d, A^d_{\rm SL})$ plane to generate the displayed predictions. Also shown are values of the current experimental measurements, the SM predictions, and the projected future experimental sensitivity. As can be seen in Fig. 7 (and also in Figs. 8 and 9 discussed later), predicted regions of the observables are significantly reduced if the constraint from γ is considered additionally.

Furthermore, results including the direct CP asymmetry, A_{CP}, in $B^- \to D^0\pi^-$ decays are discussed in what follows. It is well known that this observable can be regarded as a clean signal of NP since it vanishes in the SM. Crucially, a nonzero A_{CP} fundamentally requires the interference of at least two amplitudes possessing different weak phases and different strong phases. To obtain the prediction for A_{CP}, the PQCD expressions in Sec. IV A for evaluating the $T + C$ amplitude are used, where the necessary strong

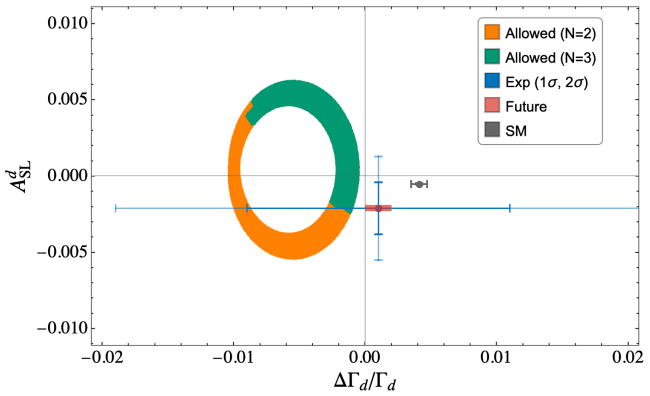


FIG. 7. The predicted regions in the $(\Delta\Gamma_d/\Gamma_d, A^d_{\rm SL})$ plane for the baseline scenario where $C^{\rm NP}_1(M_W) = 0$ [i.e., NP only enters via $C^{\rm NP}_2(M_W)$]. The blue and gray error bars represent the current experimental constraints [44,46] and the SM predictions [23], respectively. The horizontal red bands correspond to the future experimental sensitivity [25,26].

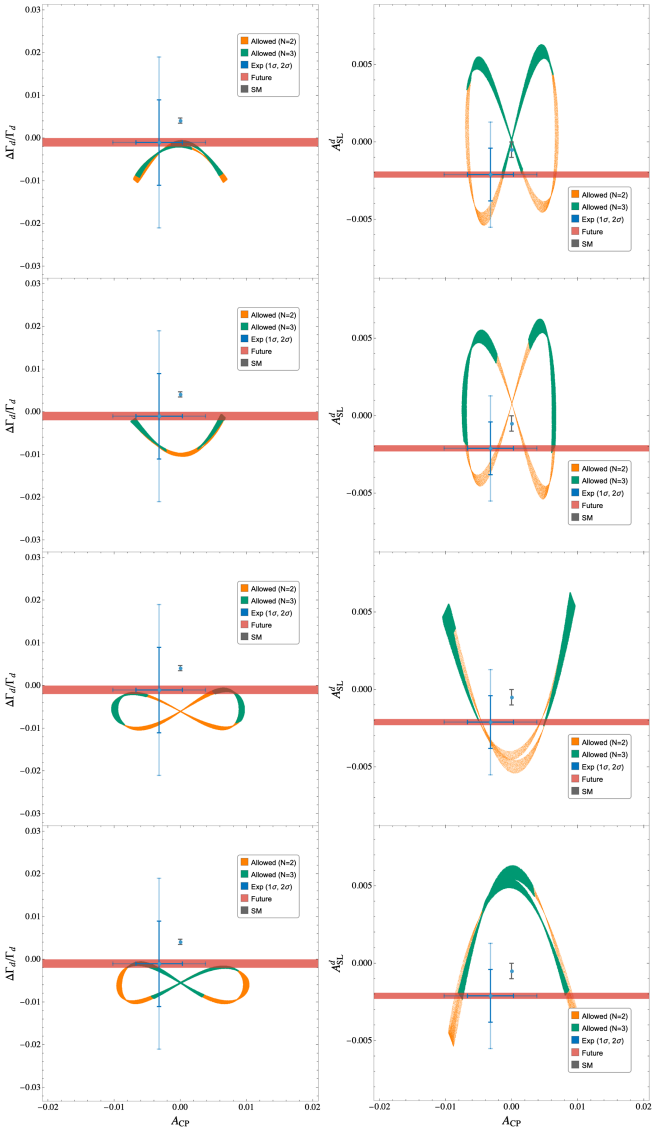


FIG. 8. The predicted regions in the ($\Delta\Gamma_d/\Gamma_d$, A_{CP}) [left column] and ($A_{\rm SL}^d$, A_{CP}) [right column] planes for four benchmark scenarios: $C_1^{\rm NP}(M_W) = 0.01,\ 0.01i,\ 0.01 + 0.01i$, and $0.01 - 0.01i$ (from top to bottom). The blue and gray error bars represent the current experimental constraints [44,46] (at the 1σ and 2σ levels) and the SM predictions [23] on the y-axis observables, respectively. The horizontal red bands correspond to the expectations for future experimental precision [25,26].

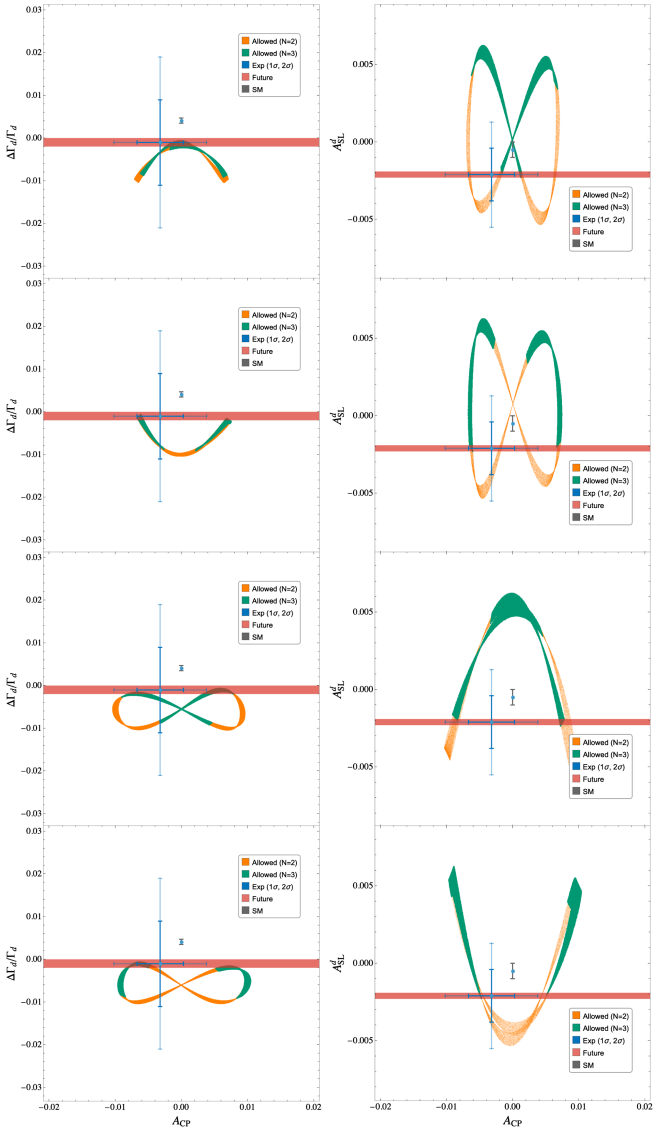


FIG. 9. The predicted regions in the ($\Delta\Gamma_d/\Gamma_d$, A_{CP}) [left column] and ($A_{\rm SL}^d$, A_{CP}) [right column] planes for four benchmark scenarios: $C_1^{\rm NP}(M_W) = -0.01, -0.01i, -0.01 + 0.01i$, and $-0.01 - 0.01i$ (from top to bottom). The blue and gray error bars represent the current experimental constraints [44,46] (at the 1σ and 2σ levels) and the SM predictions [23] on the y-axis observables, respectively. The horizontal red bands correspond to the expectations for future experimental precision [25,26].

phases are naturally generated through the decay dynamics. We find that a scenario with $C_2^{\rm NP}(M_W) \neq 0$ and $C_1^{\rm NP}(M_W) = 0$ fails to provide the necessary relative weak phase difference, yielding $A_{CP} = 0$, which we both confirmed numerically and analytically. Therefore, introducing a nonvanishing $C_1^{\rm NP}(M_W)$ is mandatory to generate the direct CP asymmetry. We focus on eight representative benchmarks: $C_1^{\rm NP}(M_W) = \pm 0.01,\ \pm 0.01i,\ \pm 0.01 \pm 0.01i$, and $\mp\, 0.01 \pm 0.01i$, which give testable size of A_{CP} in the future. The region of $C_2^{\rm NP}(M_W)$ is scanned over the possible range as was done before. We also verified that under this small variation of $C_1^{\rm NP}(M_W)$, Fig. 7 is not significantly changed. In Figs. 8 and 9, numerical predictions for A_{CP} are displayed with correlated results for the B_d^0-$\bar{B}_d^0$ mixing observables for these four selected scenarios. As illustrated in Figs. 8 and 9, a small NP contribution ($|C_1^{\rm NP}(M_W)| \sim 0.01$) produces an A_{CP} that is mostly within the 2σ range of the current PDG, while

some of the regions are outside the range. Future improvements in the experimental precision of A_{CP}, together with those for $\Delta\Gamma_d/\Gamma_d$ and A_{SL}^d, will enable us to test this NP scenario.

VI. CONCLUSION

In this work, we have performed a comprehensive analysis of the $b \to c\bar{u}q$ ($q = d, s$) transitions, aiming to address the persistent tension between the QCD factorization predictions and experimental data for color-allowed nonleptonic B meson decays. Extending the effective Hamiltonian to include complex-valued NP contributions to the Wilson coefficients C_1 and C_2, we derived constraints by analyzing the combined allowed regions from branching ratios, the CKM angle γ/ϕ_3, the lifetime ratio $\tau(B^+)/\tau(B^0)$, and neutral meson mixing observables ($\Delta\Gamma_q$ and A_{SL}^q).

For the branching ratios of the channels where amplitudes are proportional to $T + C$, the contribution of the color-suppressed diagram is model independently extracted from data, including the experimental values of branching ratios, factorization input for the ratio of T diagrams, and meson masses, as in the discussion of $T + E$ processes [12]. This method enables us to discuss constraints on the NP Wilson coefficients for the combined analysis of branching ratios and γ in a robust way. Furthermore, CP violation in $B^- \to D^0\pi^-$ decays from the CP phase of NP contributions is analyzed in the PQCD approach. With a relevant strong-phase difference determined in this method, it is shown that the direct CP violation can be $\mathcal{O}(10^{-2})$, and partially already excluded by the measurements.

Within the channels that we have studied, the combined analysis reveals a tension with the SM predictions across both $b \to c\bar{u}d$ and $b \to c\bar{u}s$ sectors. This tension manifests differently in the two channels: for the $b \to c\bar{u}d$ transition ($B_d \to D^{(*)-}\pi^+$), the SM point (i.e., $C_{i,\mathrm{NP}}(M_W) = 0$) lies outside the common 1σ allowed region. For the $b \to c\bar{u}s$ transition ($B^+ \to \bar{D}^0K^+$ and $\bar{B}_s^0 \to D_s^+K^-$), the tension is more pronounced, with the individual 1σ constraints failing to find a common region that simultaneously satisfies the experimental constraints. In both cases, this suggests that current data favors nonzero NP contributions to the tree-level current-current operators. Furthermore, the compatibility of the constraints across different decay channels points toward a potential universal NP effect governing the $b \to c\bar{u}q$ transitions, independent of $q = d, s$.

Our study reveals distinct phenomenological patterns associated with the color-singlet (C_2) and color-rearranged (C_1) scenarios. While branching ratios and the CKM angle γ provide stringent bounds on C_2^{NP}, they are comparatively less restrictive for C_1^{NP} due to $1/N_c$ suppression for the latter. Crucially, we demonstrated that the constraints from the lifetime ratio and B-$\bar{B}$ mixing observables play a decisive role in narrowing the allowed region for C_1^{NP}. In order to obtain nonzero A_{CP}, different amplitudes that have relative weak and strong phases need to interfere. It can be found that scenarios such as $C_2^{\mathrm{NP}}(M_W) \neq 0$ and $C_1^{\mathrm{NP}}(M_W) = 0$ cannot generate nonzero A_{CP}. To illustrate A_{CP} testable in the future, $C_2^{\mathrm{NP}}(M_W) = \mathcal{O}(1)$ and $C_1^{\mathrm{NP}}(M_W) = \mathcal{O}(0.01)$ are considered with some benchmark points for the latter. Based on this constrained parameter space, we provided detailed predictions for the pairwise correlations among the width difference $\Delta\Gamma_d/\Gamma_d$, the semileptonic asymmetry A_{SL}^d, and the direct CP asymmetry A_{CP}.

The precision of this theoretical framework is currently limited by hadronic uncertainties and leading-order (LO) approximations for the NP contributions. Future refinements should incorporate higher-order perturbative corrections and a more rigorous treatment of SU(3) flavor symmetry breaking. On the experimental side, the anticipated precision from the LHCb upgrade II [25,26], particularly for $\Delta\Gamma_d/\Gamma_d$ and A_{SL}^d, will be pivotal in further narrowing the NP parameter space and clarifying the tensions observed in $b \to c\bar{u}q$ decays.

ACKNOWLEDGMENTS

The work of H. U. is supported by the National Science Foundation of China under Grant No. 12405111 and the Seeds Funding of Jilin University.

DATA AVAILABILITY

There are no publicly available research data or software supporting this manuscript. Requests for further information or data should be sent to the authors.

APPENDIX A: INPUT PARAMETERS AND EXPERIMENTAL DATA

The ranges of γ denoted as $\gamma = \gamma^{\mathrm{exp}}$ in Eq. (25), measured from different decay channels are listed in Table I.

TABLE I. The ranges of γ. For $\bar{B}_s^0 \to D_s^+K^-$, two ranges are used separately. The third range is used for $B_d \to D^{*-}\pi^+$.

$B^+ \to \bar{D}^0K^+$	$8.5° < \gamma < 16.5°$ $84.5° < \gamma < 95.5°$ $163.3° < \gamma < 171.5°$	[39]
$\bar{B}_s^0 \to D_s^+K^-$	$62° < \gamma < 86°$ modulo 180° $101° < \gamma < 145°$ modulo 180°	[52] [53]
$B_d \to D^{*-}\pi^+$	$-6.96° < \gamma < 96.44°$ modulo 180° $-19.16° < \gamma < 108.64°$ modulo 180° $-5.46° < \gamma < 94.94°$ modulo 180°	[54] [55] [56]
$B^0 \to D^-\pi^+$	$5° < \gamma < 86°$ modulo 180°	[57]

TABLE II. Experimental branching ratios of different decay channels from PDG [44].

$\mathrm{Br}(B^+ \to \bar{D}^0 K^+)$	$(3.64 \pm 0.15) \times 10^{-4}$	$\mathrm{Br}(B^0 \to D^- K^+)$	$(2.05 \pm 0.08) \times 10^{-4}$
$\mathrm{Br}(\bar{B}_s^0 \to D_s^+ K^-)$	$(2.25 \pm 0.12) \times 10^{-4}$	$\mathrm{Br}(\bar{B}^0 \to D^+ K^-)$	$(2.05 \pm 0.08) \times 10^{-4}$
$\mathrm{Br}(B^0 \to D^{*-} \pi^+)$	$(2.66 \pm 0.07) \times 10^{-3}$	$\mathrm{Br}(B_s^0 \to D_s^{*-} \pi^+)$	$(1.9^{+0.5}_{-0.4}) \times 10^{-3}$
$\mathrm{Br}(B^0 \to D^- \pi^+)$	$(2.51 \pm 0.08) \times 10^{-3}$	$\mathrm{Br}(B_s^0 \to D_s^- \pi^+)$	$(2.98 \pm 0.14) \times 10^{-3}$

The branching ratios of the different decay channels used in our analysis are listed in Table II. The left column includes the main research objects, while the right columns are used only for calculating the ratios of amplitudes. Other data used in our analysis are listed in Table III. The NNLO values of a_1 are taken from Ref. [11]. Regarding the CKM input in the B^0-$\bar{B}^0$ mixing, the Wolfenstein parameters in Table III are used while $|V_{cb}|$, $|V_{ud}|$ and $|V_{us}|$ for the lifetime ratio and branching ratio analyses are from the value listed in Table III.

APPENDIX B: FORMALISM FOR B_q-$\bar{B}_q$ MIXING

1. Effective operator basis

For the analysis of B meson mixing, we employ the complete operator basis introduced in Ref. [62]:

TABLE III. Parameters used in the analysis. The values $\rho_q^i = 1$ and $\sigma_q^i = 0$ correspond to the vacuum-insertion approximation (VIA).

$F_0^{B\to D}(m_{K^-}^2)$	0.671 ± 0.011	[11]	$A_0^{B\to D^*}(m_{K^-}^2)$	0.664 ± 0.018	[11]
$F_0^{B_s\to D_s}(m_{\pi^-}^2)$	0.666 ± 0.012	[11]	$A_0^{B_s\to D_s^*}(m_{\pi^-}^2)$	0.630 ± 0.069	[11]
$\lvert a_1(D_s^+ K^-)\rvert$	$1.075^{+0.007}_{-0.011}$	[11]	$\lvert a_1(D^+ K^-)\rvert$	$1.075^{+0.007}_{-0.011}$	[11]
$\lvert a_1(D_s^{*+} \pi^-)\rvert$	$1.075^{+0.006}_{-0.011}$	[11]	$\lvert a_1(D^{*+} \pi^-)\rvert$	$1.075^{+0.006}_{-0.011}$	[11]
$\lvert a_1(D_s^+ \pi^-)\rvert$	$1.073^{+0.005}_{-0.010}$	[11]	$\lvert a_1(D^+ \pi^-)\rvert$	$1.073^{+0.005}_{-0.010}$	[11]
$f_{\pi^\pm}$	130.2 ± 0.8 MeV	[58]	$f_{K^\pm}$	155.7 ± 0.3 MeV	[58]
$\tau(B^+)$	1.638×10^{-12} s	[44]	$\tau(B^0)$	1.517×10^{-12} s	[44]
$\tau(B_s^0)$	1.516×10^{-12} s	[44]	λ	0.22501 ± 0.00068	[44]
A	$0.826^{+0.016}_{-0.015}$	[44]	$\bar{\rho}$	0.1591 ± 0.0094	[44]
$\bar{\eta}$	$0.3523^{+0.0073}_{-0.0071}$	[44]	$\lvert V_{cb}\rvert$	0.0411 ± 0.0012	[44]
$\lvert V_{ud}\rvert$	0.97367 ± 0.00032	[44]	$\lvert V_{us}\rvert$	0.22431 ± 0.00085	[44]
$\bar{B}_1(\bar{m}_b(\bar{m}_b))$	$1.013^{+0.066}_{-0.059}$	[59]	$\bar{B}_2(\bar{m}_b(\bar{m}_b))$	$1.004^{+0.085}_{-0.081}$	[59]
$\bar{\epsilon}_1(\bar{m}_b(\bar{m}_b))$	$-0.098^{+0.029}_{-0.032}$	[59]	$\bar{\epsilon}_2(\bar{m}_b(\bar{m}_b))$	$-0.037^{+0.019}_{-0.020}$	[59]
ρ_q^i	1		σ_q^i	0	
m_b^{kin}	(4.573 ± 0.012) GeV	[50]	$\bar{m}_c$ (2 GeV)	1.092 ± 0.008 GeV	[50]
$\Gamma^{\mathrm{SM}}(B^0)$	$0.636^{+0.028}_{-0.037}$ ps^{-1}	[20]	$\Gamma^{\mathrm{SM}}(B^+)$	$0.587^{+0.025}_{-0.035}$ ps^{-1}	[20]
μ_π^2	0.477 ± 0.056 GeV^2	[50]	μ_G^2	0.306 ± 0.050 GeV^2	[50]
f_{B^+}	189.4 ± 1.4 MeV	[58]	$\alpha_s(M_Z)$	0.1180 ± 0.0009	[44]
m_t^{pole}	172.4 GeV	[44]	M_W	80.3692 GeV	[44]
m_b^{pole}	4.78 GeV	[44]	$\bar{m}_b(\bar{m}_b)$	4.183 GeV	[44]
M_{B^0}	5279.72 MeV	[44]	$M_{B_s^0}$	5366.93 MeV	[44]
f_{B^0}	190.5 ± 1.3 MeV	[58]	$f_{B_s^0}$	230.7 ± 1.2 MeV	[58]
$B_{R_2}^s$	0.89 ± 0.38	[60]	$B_{R_3}^s$	1.07 ± 0.42	[60]
B_1^d	0.835 ± 0.028	[61]	B_2^d	0.791 ± 0.034	[61]
B_3^d	0.775 ± 0.054	[61]	B_4^d	1.063 ± 0.041	[61]
B_5^d	0.994 ± 0.037	[61]	η_B (4.75 GeV)	0.85 ± 0.02	[42]

$$\mathcal{O}_1^q = (\bar{b}_i q_i)_{V-A}(\bar{b}_j q_j)_{V-A}, \qquad \mathcal{O}_2^q = (\bar{b}_i q_i)_{S-P}(\bar{b}_j q_j)_{S-P},$$
$$\mathcal{O}_3^q = (\bar{b}_i q_j)_{S-P}(\bar{b}_j q_i)_{S-P}, \qquad \mathcal{O}_4^q = (\bar{b}_i q_i)_{S-P}(\bar{b}_j q_j)_{S+P},$$
$$\mathcal{O}_5^q = (\bar{b}_i q_j)_{S-P}(\bar{b}_j q_i)_{S+P}. \tag{B1}$$

The hadronic matrix elements are parametrized in terms of bag parameters as follows [42]:

$$\langle \bar{B}_q|O_1^q|B_q\rangle = \frac{8}{3} f_{B_q}^2 M_{B_q}^2 B_1^q, \qquad \langle \bar{B}_q|O_2^q|B_q\rangle = -\frac{5}{3}\frac{f_{B_q}^2 M_{B_q}^4}{(m_b+m_q)^2} B_2^q,$$
$$\langle \bar{B}_q|\mathcal{O}_3^q|B_q\rangle = \frac{1}{3}\left(\frac{m_{B_q}}{m_b+m_q}\right)^2 m_{B_q}^2 f_{B_q}^2 B_3^q, \qquad \langle \bar{B}_q|\mathcal{O}_4^q|B_q\rangle = 2\left(\frac{m_{B_q}}{m_b+m_q}\right)^2 m_{B_q}^2 f_{B_q}^2 B_4^q,$$
$$\langle \bar{B}_q|\mathcal{O}_5^q|B_q\rangle = \frac{2}{3}\left(\frac{m_{B_q}}{m_b+m_q}\right)^2 m_{B_q}^2 f_{B_q}^2 B_5^q. \tag{B2}$$

In addition to the operators $\mathcal{O}_i^q$, we also consider the four QCD operators

$$R_1^q = \frac{m_q}{m_b}(\bar{b}_i q_i)_{S-P}(\bar{b}_j q_j)_{S+P},$$
$$R_2^q = \frac{1}{m_b^2}(\bar{b}_i \overleftarrow{D}_\rho \gamma^\mu(1-\gamma_5)D^\rho q_i)(\bar{b}_j\gamma_\mu(1-\gamma_5)q_j),$$
$$R_3^q = \frac{1}{m_b^2}(\bar{b}_i \overleftarrow{D}_\rho (1-\gamma_5)D^\rho q_i)(\bar{b}_j(1-\gamma_5)q_j),$$
$$R_4^q = \frac{1}{m_b}(\bar{b}_i(1-\gamma_5)i\overleftarrow{D}_\mu q_i)(\bar{b}_j\gamma^\mu(1-\gamma_5)q_j). \tag{B3}$$

The matrix elements of these operators are parametrized as [42]

$$\langle \bar{B}_q|R_1^q|B_q\rangle = \frac{7}{3}\frac{m_q}{m_b} f_{B_q}^2 M_{B_q}^2 B_{R_1}^q,$$
$$\langle \bar{B}_q|R_2^q|B_q\rangle = -\frac{2}{3} f_{B_q}^2 M_{B_q}^2\left(\frac{M_{B_q}^2}{m_b^2}-1\right)B_{R_2}^q,$$
$$\langle \bar{B}_q|R_3^q|B_q\rangle = \frac{7}{6} f_{B_q}^2 M_{B_q}^2\left(\frac{M_{B_q}^2}{m_b^2}-1\right)B_{R_3}^q,$$
$$\langle \bar{B}_q|R_4^q|B_q\rangle = -f_{B_q}^2 M_{B_q}^2\left(\frac{M_{B_q}^2}{m_b^2}-1\right)B_{R_4}^q. \tag{B4}$$

The operators R_1^q and R_4^q are related to the basis operators $\mathcal{O}_i^q$ via the relations

$$R_1^q = \frac{m_q}{m_b}\mathcal{O}_4^q, \qquad 2R_4^q = \mathcal{O}_3^q + \mathcal{O}_1^q/2 + \mathcal{O}_2^q - 2\frac{m_q}{m_b}\mathcal{O}_5^q + R_2^q. \tag{B5}$$

2. Analytical expressions for the mixing coefficients

Adopting the formalism from Ref. [42], the general expressions for the coefficient functions D_k are decomposed into current-current (F) and penguinlike (P) contributions:

$$D_k^{uu}(\mu_2) = \sum_{i,j=1,2} C_i^*(\mu_1)C_j^*(\mu_1)F_{k,ij}^{uu}(\mu_1,\mu_2) + \frac{\alpha_s}{4\pi}(C_2^*(\mu_1))^2 P_{k,22}^{uu}(\mu_1,\mu_2) + 2\frac{\alpha_s}{4\pi}C_2^*C_{8G}^* P_{k,28}^u + 2\sum_{i=1,2}\sum_{r=3,6} C_i^* C_r^* P_{k,ir}^u,$$
$$D_k^{cu}(\mu_2) = \sum_{i,j=1,2} C_i^*(\mu_1)C_j^*(\mu_1)F_{k,ij}^{cu}(\mu_1,\mu_2) + \frac{\alpha_s}{4\pi}(C_2^*(\mu_1))^2 P_{k,22}^{cu}(\mu_1,\mu_2) + \frac{\alpha_s}{4\pi}C_2^*C_{8G}^*(P_{k,28}^c + P_{k,28}^u)$$
$$+ \sum_{i=1,2}\sum_{r=3,6} C_i^* C_r^*(P_{k,ir}^c + P_{k,ir}^u),$$
$$D_k^{cc}(\mu_2) = \sum_{i,j=1,2} C_i^*(\mu_1)C_j^*(\mu_1)F_{k,ij}^{cc}(\mu_1,\mu_2) + \frac{\alpha_s}{4\pi}(C_2^*(\mu_1))^2 P_{k,22}^{cc}(\mu_1,\mu_2) + 2\frac{\alpha_s}{4\pi}C_2^*C_{8G}^* P_{k,28}^c + 2\sum_{i=1,2}\sum_{r=3,6} C_i^* C_r^* P_{k,ir}^c. \tag{B6}$$

It should be noted that complex conjugate is taken for the Wilson coefficients for our convention in Eq. (1). In this work, we restrict the calculation of contributions induced by NP to LO accuracy, and discard the penguin contributions represented by

the P terms and focus on the current-current functions $F^{qq'}_{k,ij}$. The perturbative expansion of these functions is formally written as

$$F^{qq'}_{k,ij} = A^{qq'}_{k,ij} + \frac{\alpha_s}{4\pi} B^{qq'}_{k,ij}, \tag{B7}$$

where the indices (qq') run over $\{(uu),(cu),(cc)\}$. To maintain consistency with the LO approximation, we retain only the zeroth-order coefficients $A^{qq'}_{k,ij}$ and neglect the $\mathcal{O}(\alpha_s)$ corrections $B^{qq'}_{k,ij}$.

The analytical forms for the relevant $A^{qq'}_{k,ij}$ coefficients are listed below. They are expressed in terms of the mass ratio $z = m_c^2/m_b^2$. We note that the coefficients for the uu sector can be derived directly from the cc sector by taking the massless charm limit ($m_c \to 0$) [42].

$$\begin{aligned}
A^{cu}_{1,11} &= \frac{3}{2}(2-3z+z^3), & A^{cu}_{2,11} &= 3(1-z)^2(1+2z),\\
A^{cu}_{1,12} &= \frac{1}{2}(2-3z+z^3), & A^{cu}_{2,12} &= (1-z)^2(1+2z),\\
A^{cu}_{1,22} &= \frac{1}{2}(1-z)^3, & A^{cu}_{2,22} &= -(1-z)^2(1+2z),\\
A^{cc}_{1,11} &= 3\sqrt{1-4z}(1-z), & A^{cc}_{2,11} &= 3\sqrt{1-4z}(1+2z),\\
A^{cc}_{1,12} &= \sqrt{1-4z}(1-z), & A^{cc}_{2,12} &= \sqrt{1-4z}(1+2z),\\
A^{cc}_{1,22} &= \frac{1}{2}(1-4z)^{3/2}, & A^{cc}_{2,22} &= -\sqrt{1-4z}(1+2z).
\end{aligned} \tag{B8}$$

Finally, we incorporate the $1/m_b$ power corrections through the parameters $\delta^{qq',q}_{1/m}$. These corrections depend on the matrix elements of the dimension-7 operators and coefficients $K_{1,2}$, defined as follows [42]:

$$\begin{aligned}
\delta^{ccq}_{1/m} &= \sqrt{1-4z}\left((1+2z)\left[K_2(\langle R^q_2\rangle + 2\langle R^q_4\rangle) - 2K_1(\langle R^q_1\rangle + \langle R^q_2\rangle)\right] - \frac{12z^2}{1-4z}\left[K_1(\langle R^q_2\rangle + 2\langle R^q_3\rangle) + 2K_2\langle R^q_3\rangle\right]\right),\\
\delta^{cuq}_{1/m} &= (1-z)^2\left((1+2z)\left[K_2(\langle R^q_2\rangle + 2\langle R^q_4\rangle) - 2K_1(\langle R^q_1\rangle + \langle R^q_2\rangle)\right] - \frac{6z^2}{(1-z)^2}(K_1(\langle R^q_2\rangle + 2\langle R^q_3\rangle) + 2K_2\langle R^q_3\rangle)\right),\\
\delta^{uuq}_{1/m} &= \left[K_2(\langle R^q_2\rangle + 2\langle R^q_4\rangle) - 2K_1(\langle R^q_1\rangle + \langle R^q_2\rangle)\right],
\end{aligned} \tag{B9}$$

where $\langle R^q_i\rangle = \langle \bar{B}_q | R^q_i | B_q\rangle$ and the combinations $K_{1,2}$ are determined by the $\Delta B = 1$ Wilson coefficients:

$$K_1 = 3C_1^{*2} + 2\mathrm{Re}(C_1^* C_2^*), \qquad K_2 = C_2^{*2}. \tag{B10}$$

APPENDIX C: FORMULAS FOR $B \to D\pi$ IN PQCD

In this Appendix, we collect the explicit PQCD expressions for the building blocks entering the class-III amplitude $B^- \to D^0\pi^-$ in Eq. (32). Unless specified otherwise, the formulas, definitions, and conventions in this Appendix are compiled from Ref. [45], to which we refer the reader for further details. Only the quantities used in the direct CP analysis are listed below, including the factorizable amplitudes, nonfactorizable amplitudes, hard kernels, evolution factors, and meson distribution amplitudes.

We use the light-cone momentum assignment

$$P_1 = \frac{m_B}{\sqrt{2}}(1,1,\mathbf{0}_T), \tag{C1}$$

$$P_2 = \frac{m_B}{\sqrt{2}}(1,r^2,\mathbf{0}_T), \tag{C2}$$

$$P_3 = \frac{m_B}{\sqrt{2}}(0,1-r^2,\mathbf{0}_T), \tag{C3}$$

where P_1, P_2 and P_3 denote the momenta of the B, D and π mesons, respectively. The shorthand notations are

$$r = \frac{m_D}{m_B}, \qquad r_0 = \frac{m_0}{m_B}, \qquad [dx] = dx_1 dx_2 dx_3, \tag{C4}$$

where $m_0 = 1.4$ GeV is the chiral enhancement scale for the pion twist-3 distribution amplitudes. The variables x_i denote the longitudinal momentum fractions of the light partons in the corresponding mesons, and b_i are the impact parameters conjugate to the transverse momenta. We also use

$$N = N_c = 3, \qquad C_F = \frac{N_c^2-1}{2N_c} = \frac{4}{3}. \tag{C5}$$

The effective combinations of Wilson coefficients are

$$a_1(t) = C_2(t) + \frac{C_1(t)}{N_c}, \qquad a_2(t) = C_1(t) + \frac{C_2(t)}{N_c}. \tag{C6}$$

In the presence of NP, the coefficients $C_{1,2}(t)$ appearing below are understood as the low-scale Wilson coefficients obtained after RGE evolution from the boundary values at M_W.

The factorizable external and internal emission amplitudes are

$$\xi_{\rm ext} = 16\pi C_F\sqrt{r}m_B^2\int_0^1 dx_1dx_2\int_0^{1/\Lambda} b_1db_1b_2db_2\phi_B(x_1,b_1)\phi_D(x_2) \times\left[E_e(t_e^{(1)})h(x_1,x_2,b_1,b_2)S_t(x_2)+rE_e(t_e^{(2)})h(x_2,x_1,b_2,b_1)S_t(x_1)\right], \tag{C7}$$

$$\begin{aligned}\xi_{\rm int} = 16\pi C_F\sqrt{r}m_B^2\int_0^1 dx_1dx_3\int_0^{1/\Lambda} b_1db_1b_3db_3\phi_B(x_1,b_1) &\times\Big\{[(1+x_3)\phi_\pi(x_3)+r_0(1-2x_3)(\phi_\pi^p(x_3)+\phi_\pi^t(x_3))] \\ &\times E_i(t_i^{(1)})h(x_1,x_3(1-r^2),b_1,b_3)S_t(x_3) \\ &+2r_0\phi_\pi^p(x_3)E_i(t_i^{(2)})h(x_3,x_1(1-r^2),b_3,b_1)S_t(x_1)\Big\}.\end{aligned} \tag{C8}$$

The corresponding evolution factors are

$$E_e(t) = \alpha_s(t)a_1(t)\exp[-S_B(t)-S_D(t)], \tag{C9}$$

$$E_i(t) = \alpha_s(t)a_2(t)\exp[-S_B(t)-S_\pi(t)]. \tag{C10}$$

The nonfactorizable amplitudes are

$$\mathcal{M}_{\rm ext} = 32\pi\sqrt{2N}C_F\sqrt{r}m_B^2\int_0^1[dx]\int_0^{1/\Lambda} b_1db_1b_3db_3\phi_B(x_1,b_1)\phi_D(x_2)\phi_\pi(x_3) \times\left[x_3E_b(t_b^{(1)})h_b^{(1)}(x_i,b_i)-(1-x_3+x_2)E_b(t_b^{(2)})h_b^{(2)}(x_i,b_i)\right], \tag{C11}$$

$$\mathcal{M}_{\rm int} = 32\pi\sqrt{2N}C_F\sqrt{r}m_B^2\int_0^1[dx]\int_0^{1/\Lambda} b_1db_1b_2db_2\phi_B(x_1,b_1)\phi_D(x_2) \times\left[(-x_2-x_3)\phi_\pi(x_3)E_d(t_d^{(1)})h_d^{(1)}(x_i,b_i)+(1-x_2)\phi_\pi(x_3)E_d(t_d^{(2)})h_d^{(2)}(x_i,b_i)\right]. \tag{C12}$$

The evolution factors for the nonfactorizable terms are

$$E_b(t) = \alpha_s(t)\frac{C_1(t)}{N_c}\exp\left[-S(t)|_{b_2=b_1}\right], \tag{C13}$$

$$E_d(t) = \alpha_s(t)\frac{C_2(t)}{N_c}\exp\left[-S(t)|_{b_3=b_1}\right], \tag{C14}$$

with

$$S(t) = S_B(t)+S_D(t)+S_\pi(t). \tag{C15}$$

The hard functions entering the factorizable amplitudes are

$$\begin{aligned}h(x_1,x_2,b_1,b_2) &= K_0(\sqrt{x_1x_2}m_Bb_1) \\ &\times\left[\theta(b_1-b_2)K_0(\sqrt{x_2}m_Bb_1)I_0(\sqrt{x_2}m_Bb_2)\right. \\ &\left.+\theta(b_2-b_1)K_0(\sqrt{x_2}m_Bb_2)I_0(\sqrt{x_2}m_Bb_1)\right].\end{aligned} \tag{C16}$$

For the nonfactorizable amplitudes, the hard functions are

$$\begin{aligned}h_b^{(j)}(x_i,b_i) = &\left[\theta(b_1-b_3)K_0(Bm_Bb_1)I_0(Bm_Bb_3)+\theta(b_3-b_1)K_0(Bm_Bb_3)I_0(Bm_Bb_1)\right] \\ &\times\begin{cases}K_0(B_jm_Bb_3), & B_j^2\geq 0,\\ \frac{i\pi}{2}H_0^{(1)}\left(\sqrt{|B_j^2|}m_Bb_3\right), & B_j^2\leq 0,\end{cases}\end{aligned} \tag{C17}$$

$$h_d^{(j)}(x_i,b_i)=\left[\theta(b_1-b_2)K_0(Dm_Bb_1)I_0(Dm_Bb_2)+\theta(b_2-b_1)K_0(Dm_Bb_2)I_0(Dm_Bb_1)\right]\times\begin{cases}K_0(D_jm_Bb_2), & D_j^2\geq 0,\\ \frac{i\pi}{2}H_0^{(1)}\left(\sqrt{|D_j^2|}m_Bb_2\right), & D_j^2\leq 0.\end{cases}\tag{C18}$$

Here $j=1,2$, K_0 and I_0 are modified Bessel functions, $H_0^{(1)}$ is the Hankel function of the first kind, and θ is the step function. The variables entering these functions are

$$B^2=x_1x_2,\tag{C19}$$

$$B_1^2=x_1x_2-x_2x_3(1-r^2),\tag{C20}$$

$$B_2^2=x_1x_2-x_2(1-x_3)(1-r^2),\tag{C21}$$

$$D^2=x_1x_3(1-r^2),\tag{C22}$$

$$D_1^2=(x_1-x_2)x_3(1-r^2),\tag{C23}$$

$$D_2^2=(x_1+x_2)r^2-(1-x_1-x_2)x_3(1-r^2).\tag{C24}$$

The hard scales are chosen as

$$t_e^{(1)}=\max\left(\sqrt{x_2}m_B,\frac{1}{b_1},\frac{1}{b_2}\right),\qquad t_e^{(2)}=\max\left(\sqrt{x_1}m_B,\frac{1}{b_1},\frac{1}{b_2}\right),\tag{C25}$$

$$t_i^{(1)}=\max\left(\sqrt{x_3(1-r^2)}m_B,\frac{1}{b_1},\frac{1}{b_3}\right),\qquad t_i^{(2)}=\max\left(\sqrt{x_1(1-r^2)}m_B,\frac{1}{b_1},\frac{1}{b_3}\right),\tag{C26}$$

$$t_b^{(j)}=\max\left(Bm_B,\sqrt{|B_j^2|}m_B,\frac{1}{b_1},\frac{1}{b_3}\right),\qquad t_d^{(j)}=\max\left(Dm_B,\sqrt{|D_j^2|}m_B,\frac{1}{b_1},\frac{1}{b_2}\right).\tag{C27}$$

The meson distribution amplitudes used in the calculation are

$$\phi_B(x,b)=N_Bx^2(1-x)^2\exp\left[-\frac{1}{2}\left(\frac{xm_B}{\omega_B}\right)^2-\frac{\omega_B^2b^2}{2}\right],\tag{C28}$$

$$\phi_D(x)=\frac{3}{\sqrt{2N_c}}f_Dx(1-x)[1+C_D(1-2x)],\tag{C29}$$

$$\phi_\pi(x)=\frac{3f_\pi}{\sqrt{2N_c}}x(1-x)[1+0.44C_2^{3/2}(2x-1)+0.25C_4^{3/2}(2x-1)],\tag{C30}$$

$$\phi_\pi^p(x)=\frac{f_\pi}{2\sqrt{2N_c}}[1+0.43C_2^{1/2}(2x-1)+0.09C_4^{1/2}(2x-1)],\tag{C31}$$

$$\phi_\pi^t(x)=\frac{f_\pi}{2\sqrt{2N_c}}(1-2x)[1+0.55(10x^2-10x+1)].\tag{C32}$$

The normalization constant N_B is fixed by

$$\int_0^1 dx\phi_B(x,0)=\frac{f_B}{2\sqrt{2N_c}}.\tag{C33}$$

The shape parameters are taken as

$$\omega_B=0.4\ \text{GeV},\qquad C_D=0.8\pm0.2,\tag{C34}$$

and the infrared cutoff is chosen as

$$\Lambda = \Lambda^{(4)}_{\rm QCD} = 0.25\ {\rm GeV}. \tag{C35}$$

For the Gegenbauer polynomials, we define $z = 2x - 1$ and use

$$C_2^{1/2}(z) = \frac{1}{2}(3z^2 - 1), \qquad C_4^{1/2}(z) = \frac{1}{8}(35z^4 - 30z^2 + 3), \tag{C36}$$

$$C_2^{3/2}(z) = \frac{3}{2}(5z^2 - 1), \qquad C_4^{3/2}(z) = \frac{15}{8}(21z^4 - 14z^2 + 1). \tag{C37}$$

The threshold resummation factor is parametrized as

$$S_t(x) = \frac{2^{1+2c}\Gamma(3/2+c)}{\sqrt{\pi}\Gamma(1+c)}[x(1-x)]^c, \qquad c = 0.35. \tag{C38}$$

The Sudakov exponents are [63,64]

$$S_B(t) = s(x_1 P_1^+, b_1) + 2\int_{1/b_1}^{t} \frac{d\mu'}{\mu'}\gamma_q(\mu'), \tag{C39}$$

$$S_D(t) = s(x_2 P_2^+, b_2) + 2\int_{1/b_2}^{t} \frac{d\mu'}{\mu'}\gamma_q(\mu'), \tag{C40}$$

$$S_\pi(t) = s(x_3 P_3^-, b_3) + s((1-x_3)P_3^-, b_3) + 2\int_{1/b_3}^{t} \frac{d\mu'}{\mu'}\gamma_q(\mu'). \tag{C41}$$

The exponent $s(Q, b)$ is given by [64]

$$s(Q,b) = \int_{1/b}^{Q} \frac{d\mu'}{\mu'}\left[\left\{\frac{2}{3}(2\gamma_E - 1 - \ln 2) + C_F \ln\frac{Q}{\mu'}\right\} \times \frac{\alpha_s(\mu')}{\pi} + \left\{\frac{67}{9} - \frac{\pi^2}{3} - \frac{10}{27}n_f + \frac{2}{3}\beta_0 \ln\frac{\gamma_E}{2}\right\} \times \left(\frac{\alpha_s(\mu')}{\pi}\right)^2 \ln\frac{Q}{\mu'}\right], \tag{C42}$$

where

$$\gamma_q(\mu') = -\frac{\alpha_s(\mu')}{\pi}, \qquad \beta_0 = 11 - \frac{2}{3}n_f, \qquad n_f = 4. \tag{C43}$$

Here γ_E denotes Euler's constant.

[1] M. Beneke, G. Buchalla, M. Neubert, and C. T. Sachrajda, QCD factorization for exclusive, nonleptonic B meson decays: General arguments and the case of heavy light final states, Nucl. Phys. **B591**, 313 (2000).

[2] T. Huber, S. Kränkl, and X.-Q. Li, Two-body non-leptonic heavy-to-heavy decays at NNLO in QCD factorization, J. High Energy Phys. 09 (2016) 112.

[3] M. Bordone, N. Gubernari, T. Huber, M. Jung, and D. van Dyk, A puzzle in $\bar{B}^0_{(s)} \to D^{(*)+}_{(s)}\{\pi^-, K^-\}$ decays and extraction of the f_s/f_d fragmentation fraction, Eur. Phys. J. C **80**, 951 (2020).

[4] M. L. Piscopo and A. V. Rusov, Non-factorisable effects in the decays $\bar{B}^0_s \to D^+_s\pi^-$ and $\bar{B}^0 \to D^+K^-$ from LCSR, J. High Energy Phys. 10 (2023) 180.

[5] M. Endo, S. Iguro, and S. Mishima, Revisiting rescattering contributions to $\bar{B}_{(s)} \to D^{(*)}_{(s)}M$ decays, J. High Energy Phys. 01 (2022) 147.

[6] C.-K. Chua, W.-S. Hou, and K.-C. Yang, Final state rescattering and color suppressed $B^0 \to D^{(*)0}h^0$ decays, Phys. Rev. D **65**, 096007 (2002).

[7] C.-K. Chua and W.-S. Hou, Implications of $\bar{B}^0 \to D^0\pi^0$ decays on $\bar{B} \to D\bar{K}$, $\bar{D}\,\bar{K}$ decays, Phys. Rev. D **72**, 036002 (2005).

[8] C.-K. Chua and W.-S. Hou, Rescattering effects in $\bar{B}_{u,d,s} \to DP, \bar{D}P$ decays, Phys. Rev. D **77**, 116001 (2008).

[9] C.-K. Chua, Revisiting final state interaction in charmless $B_q \to PP$ decays, Phys. Rev. D **97**, 093004 (2018).

[10] S. Iguro and T. Kitahara, Implications for new physics from a novel puzzle in $\bar{B}^0_{(s)} \to D^{(*)+}_{(s)}\{\pi^-, K^-\}$ decays, Phys. Rev. D **102**, 071701 (2020).

[11] F.-M. Cai, W.-J. Deng, X.-Q. Li, and Y.-D. Yang, Probing new physics in class-I B-meson decays into heavy-light final states, J. High Energy Phys. 10 (2021) 235.

[12] R. Fleischer and E. Malami, Using $B^0_s \to D^\mp_s K^\pm$ decays as a portal to new physics, Phys. Rev. D **106**, 056004 (2022).

[13] A. Lenz, J. Müller, M. L. Piscopo, and A. V. Rusov, Taming new physics in $b \to c\bar{u}d(s)$ with $\tau(B^+)/\tau(B_d)$ and a^d_{sl}, J. High Energy Phys. 09 (2023) 028.

[14] A. H. Panuluh, S. Tanaka, and H. Umeeda, $B_{(s)} \to D^{(*)}_{(s)}M$ decays in the presence of final-state interactions, Phys. Rev. D **111**, 095020 (2025).

[15] S. Meiser, D. van Dyk, and J. Virto, Towards a global analysis of the $b \to c\bar{u}q$ puzzle, J. High Energy Phys. 06 (2025) 019.

[16] O. Atkinson, C. Englert, M. Kirk, and G. Tetlalmatzi-Xolocotzi, Collider-flavour complementarity from the bottom to the top, Eur. Phys. J. C **85**, 258 (2025).

[17] J. Y. Araz, C. Englert, M. Kirk, and G. Tetlalmatzi-Xolocotzi, New insights into the $b \to c\bar{u}q$ puzzle through Top-Bottom synergies, Eur. Phys. J. C **86**, 1045 (2026).

[18] H.-Y. Cheng, Phenomenological study of heavy hadron lifetimes, J. High Energy Phys. 11 (2018) 014.
[19] A. Lenz, M. L. Piscopo, and A. V. Rusov, Disintegration of beauty: A precision study, J. High Energy Phys. 01 (2023) 004.
[20] M. Egner, M. Fael, A. Lenz, M. L. Piscopo, A. V. Rusov, K. Schönwald, and M. Steinhauser, Total decay rates of B mesons at NNLO-QCD, J. High Energy Phys. 04 (2025) 106.
[21] M. Lang, A. Lenz, A. Mohamed, M. L. Piscopo, and A. V. Rusov, B-meson decay width up to $1/m_b^3$ corrections within and beyond the Standard Model, J. High Energy Phys. 05 (2026) 100.
[22] C. Bobeth, U. Haisch, A. Lenz, B. Pecjak, and G. Tetlalmatzi-Xolocotzi, On new physics in $\Delta\Gamma_d$, J. High Energy Phys. 06 (2014) 040.
[23] J. Albrecht, F. Bernlochner, A. Lenz, and A. Rusov, Lifetimes of b-hadrons and mixing of neutral B-mesons: Theoretical and experimental status, Eur. Phys. J. Special Topics **233**, 359 (2024).
[24] U. Nierste, P. Reeck, V. Shtabovenko, and M. Steinhauser, Complete next-to-next-to-leading order QCD corrections to the decay matrix in B-meson mixing at leading power, J. High Energy Phys. 03 (2026) 094.
[25] R. Aaij *et al.* (LHCb Collaboration), Physics case for an LHCb upgrade II—Opportunities in flavour physics, and beyond, in the HL-LHC era, arXiv:1808.08865.
[26] A. Cerri *et al.*, Report from working group 4: Opportunities in flavour physics at the HL-LHC and HE-LHC, CERN Yellow Rep. Monogr. **7**, 867 (2019).
[27] J. Brod, A. Lenz, G. Tetlalmatzi-Xolocotzi, and M. Wiebusch, New physics effects in tree-level decays and the precision in the determination of the quark mixing angle γ, Phys. Rev. D **92**, 033002 (2015).
[28] A. Lenz and G. Tetlalmatzi-Xolocotzi, Model-independent bounds on new physics effects in non-leptonic tree-level decays of B-mesons, J. High Energy Phys. 07 (2020) 177.
[29] R. Fleischer, New strategies to obtain insights into CP violation through $B_s \to D_s^{\pm} K^{\mp}$, $D_s^{*\pm} K^{\mp}$,... and $B_d \to D^{\pm}\pi^{\mp}$, $D^{*\pm}\pi^{\mp}$,... decays, Nucl. Phys. **B671**, 459 (2003).
[30] M. Gronau and D. London, How to determine all the angles of the unitarity triangle from $B_d{}^0 \to DK_s$ and $B_s{}^0 \to D_\varphi$, Phys. Lett. B **253**, 483 (1991).
[31] M. Gronau and D. Wyler, On determining a weak phase from CP asymmetries in charged B decays, Phys. Lett. B **265**, 172 (1991).
[32] D. Atwood, I. Dunietz, and A. Soni, Enhanced CP violation with $B \to KD^0(\bar{D}^0)$ modes and extraction of the CKM angle γ, Phys. Rev. Lett. **78**, 3257 (1997).
[33] D. Atwood, I. Dunietz, and A. Soni, Improved methods for observing CP Violation in $B^{\pm} \to KD$ and measuring the CKM phase γ, Phys. Rev. D **63**, 036005 (2001).
[34] R. Fleischer and E. Malami, Revealing new physics in $B_s^0 \to D_s^{\mp} K^{\pm}$ decays, Eur. Phys. J. C **83**, 420 (2023).
[35] R. Aaij *et al.* (LHCb Collaboration), First Measurement of the decay-time-integrated CP asymmetry in $B_s^0 \to D_s^- \pi^+$ decays, Phys. Rev. Lett. **137**, 081802 (2026).
[36] T. Gershon, A. Lenz, A. V. Rusov, and N. Skidmore, Testing the Standard Model with CP asymmetries in flavor-specific nonleptonic decays, Phys. Rev. D **105**, 115023 (2022).
[37] K. Abe *et al.* (Belle Collaboration), Study of $B^{\pm} \to D_{CP} K^{\pm}$ and $D_{CP}^* K^{\pm}$ decays, Phys. Rev. D **73**, 051106 (2006).
[38] T. Bloomfield *et al.* (Belle Collaboration), Measurement of the branching fraction and CP asymmetry for $B \to \bar{D}^0\pi$ decays, Phys. Rev. D **105**, 072007 (2022).
[39] I. Adachi *et al.* (Belle, Belle-II Collaborations), Measurement of branching-fraction ratios and CP asymmetries in $B^{\pm} \to D_{CP\pm} K^{\pm}$ decays at Belle and Belle II, J. High Energy Phys. 05 (2024) 212.
[40] R. Aaij *et al.* (LHCb Collaboration), Observation of the suppressed ADS modes $B^{\pm} \to [\pi^{\pm} K^{\mp} \pi^+ \pi^-]_D K^{\pm}$ and $B^{\pm} \to [\pi^{\pm} K^{\mp} \pi^+ \pi^-]_D \pi^{\pm}$, Phys. Lett. B **723**, 44 (2013).
[41] G. Buchalla, A. J. Buras, and M. E. Lautenbacher, Weak decays beyond leading logarithms, Rev. Mod. Phys. **68**, 1125 (1996).
[42] M. Ciuchini, E. Franco, V. Lubicz, F. Mescia, and C. Tarantino, Lifetime differences and CP violation parameters of neutral B mesons at the next-to-leading order in QCD, J. High Energy Phys. 08 (2003) 031.
[43] T. Inami and C. S. Lim, Effects of superheavy quarks and leptons in low-energy weak processes $K_L \to \mu\bar{\mu}$, $K^+ \to \pi^+ \nu\bar{\nu}$ and $K^0 \leftrightarrow \bar{K}^0$, Prog. Theor. Phys. **65**, 297 (1981); **65**, 1772(E) (1981).
[44] S. Navas *et al.* (Particle Data Group), Review of particle physics, Phys. Rev. D **110**, 030001 (2024).
[45] Y.-Y. Keum, T. Kurimoto, H. N. Li, C.-D. Lu, and A. I. Sanda, Nonfactorizable contributions to $B \to D^{(*)} M$ decays, Phys. Rev. D **69**, 094018 (2004).
[46] S. Banerjee *et al.* (Heavy Flavor Averaging Group (HFLAV) Collaboration), Averages of b-hadron, c-hadron, and τ-lepton properties as of 2023, Phys. Rev. D **113**, 012008 (2026).
[47] HFLAV Collaboration, Summer 2025 updates, https://hflav.web.cern.ch/ (2025).
[48] J. Charles *et al.*, Current status of the Standard Model CKM fit and constraints on $\Delta F = 2$ New Physics, Phys. Rev. D **91**, 073007 (2015).
[49] CKMfitter Group, CKMfitter global CKM fit results: Summer 2025, https://ckmfitter.in2p3.fr/ (2025), numerical results from the CKMfitter global analysis, accessed July 2026.
[50] M. Bordone, B. Capdevila, and P. Gambino, Three loop calculations and inclusive V_{cb}, Phys. Lett. B **822**, 136679 (2021).
[51] K. G. Chetyrkin, J. H. Kuhn, and M. Steinhauser, RunDec: A Mathematica package for running and decoupling of the strong coupling and quark masses, Comput. Phys. Commun. **133**, 43 (2000).
[52] R. Aaij *et al.* (LHCb Collaboration), Measurement of CP asymmetry in $B_s^0 \to D_s^{\mp} K^{\pm}$ decays, J. High Energy Phys. 03 (2018) 059.
[53] R. Aaij *et al.* (LHCb Collaboration), Measurement of CP asymmetry in $B_s^0 \to D_s^{\mp} K^{\pm}$ decays, J. High Energy Phys. 03 (2025) 139.
[54] B. Aubert *et al.* (*BABAR* Collaboration), Measurement of time-dependent CP-violating asymmetries and constraints

on $(2\beta + \gamma)$ with partial reconstruction of $B \to D^{*\mp}\pi^{\pm}$ decays, Phys. Rev. D **71**, 112003 (2005).

[55] F. J. Ronga *et al.* (Belle Collaboration), Measurements of CP violation in $B^0 \to D^{*-}\pi^+$ and $B^0 \to D^-\pi^+$ decays, Phys. Rev. D **73**, 092003 (2006).

[56] B. Aubert *et al.* (*BABAR* Collaboration), Measurement of time-dependent CP asymmetries in $B^0 \to D^{(*)\pm}\pi^{\mp}$ and $B^0 \to D^{\pm}\rho^{\mp}$ decays, Phys. Rev. D **73**, 111101 (2006).

[57] R. Aaij *et al.* (LHCb Collaboration), Measurement of CP violation in $B^0 \to D^{\mp}\pi^{\pm}$ decays, J. High Energy Phys. 06 (2018) 084.

[58] Y. Aoki *et al.* (Flavour Lattice Averaging Group (FLAG) Collaboration), FLAG review 2024, Phys. Rev. D **113**, 014508 (2026).

[59] M. Black, M. Lang, A. Lenz, and Z. Wüthrich, HQET sum rules for matrix elements of dimension-six four-quark operators for meson lifetimes within and beyond the Standard Model, J. High Energy Phys. 04 (2025) 081.

[60] C. T. H. Davies, J. Harrison, G. P. Lepage, C. J. Monahan, J. Shigemitsu, and M. Wingate (HPQCD Collaboration), Lattice QCD matrix elements for the $B_s^0 - \bar{B}_s^0$ width difference beyond leading order, Phys. Rev. Lett. **124**, 082001 (2020).

[61] L. Di Luzio, M. Kirk, A. Lenz, and T. Rauh, ΔM_s theory precision confronts flavour anomalies, J. High Energy Phys. 12 (2019) 009.

[62] D. Becirevic, V. Gimenez, G. Martinelli, M. Papinutto, and J. Reyes, B-parameters of the complete set of matrix elements of $(\Delta B = 2)$ operators from the lattice, J. High Energy Phys. 04 (2002) 025.

[63] Y. Y. Keum, H.-N. Li, and A. I. Sanda, Penguin enhancement and $B \to K\pi$ decays in perturbative QCD, Phys. Rev. D **63**, 054008 (2001).

[64] C.-D. Lu and K. Ukai, Branching ratios of $B \to D_s K$ decays in perturbative QCD approach, Eur. Phys. J. C **28**, 305 (2003).